Techno-economic analyses of CO_2 liquefaction: Impact of product pressure and impurities

Han Deng[a], Simon Roussanaly[a,*], and Geir Skaugen[a]

[a]*SINTEF Energy Research, Sem Sælandsvei 11, NO-7465 Trondheim, Norway*

* Corresponding author. Tel.: +47 47441763; E-mail address: simon.roussanaly@sintef.no

Abstract

As a first step towards identifying the optimal transport conditions for shipping CO_2, this study investigates the impact of post-liquefaction delivery pressure on the design and cost of CO_2 liquefaction for (a) pure CO_2 (b) three impurity scenarios (c) two purity requirements.
For pure CO_2, the highest liquefaction cost is obtained at 7 bar amongst the range considered (7 to 70 bar), while a minimum lies around 40-50 bar. When different potential impurity scenarios are considered, impurities need to be purged for the low-pressure cases as these are not necessarily soluble in the liquefied CO_2 stream. As a consequence, the liquefaction cost increases significantly for low-pressure cases (up to 34% compared to the pure CO_2), and wider differences between the pressure levels are obtained. Purity requirements also have a significant impact on comparisons of delivery pressures, although this impact depends on both the impurities present and the purity requirement considered.

Keywords: Carbon Capture and Storage (CCS); CO_2 transport; CO_2 liquefaction; Impurities; Techno-economic analysis.

Nomenclature

A	heat exchange area, [m^2]
C	concentration in mole fraction, [-]
h	specific enthalpy, [J kg^{-1}]
$\dot{m}$	mass flow rate, [kg s^{-1}]
P	pressure, [bar]
T	temperature, [°C]
ΔT	temperature difference, [°C]
ΔT_{sub}	subcooled temperature, [°C]
ΔT_{sup}	superheated temperature, [°C]
U	overall heat transfer coefficient [W m^{-2} K^{-1}]
W	power [W]

Greek symbols

η_{is}	isentropic efficiency, [-]
η_{motor}	motor efficiency, [-]

Subscripts

imp	impurity
liq	liquefier or liquefaction
min	minimum value
ref	refrigerant
sink	heat sink, cooling water

Abbreviations

CCS	carbon capture and storage
CEPCI	chemical engineering plant cost index

This is the accepted version of an article published in International Journal of Refrigeration
DOI: 10.1016/j.ijrefrig.2019.04.011

DC direct cost
IEA International Energy Agency
LPG liquefied petroleum gas
NLPQL non-linear programming by quadratic lagrangian
TDC total direct cost
TDCPC total direct cost including process contingency
TPC total plant cost

1 Introduction

Carbon Capture and Storage (CCS) is expected to contribute to 14% of the decarbonisation of both power sector and industrial emissions (International Energy Agency, 2013, 2016). For this ambition to be realised, the costs of CO_2 capture and storage will need to be reduced through development of CO_2 capture technologies (Størset et al., 2019), such as solvents (Mota-Martinez et al., 2017), membranes (Roussanaly et al., 2018), low-temperature processes (Berstad et al., 2013), as well as demonstration projects (Herzog, 2011). In addition, CO_2 shall be transported from sources to sinks in a cost-effective and safe way (Roussanaly et al., 2014; Roussanaly et al., 2013b).

While pipeline transport has traditionally been treated as the best option for CO_2 transport due to its low cost for short distances and important economies of scale, interest in vessel-based transport of CO_2 is rising. Indeed, ship transport is more cost-efficient than pipelines for long distances and small volumes, requires less investment, is more flexible, requires less construction time (Roussanaly et al., 2013a) and offers opportunities for co-utilisation of infrastructure (Aspelund et al., 2009). These advantages make ship-based transport of CO_2 an attractive technology for early deployment of CCS, as for example in the Norwegian full-scale CCS project (Ministry of Petroleum and Energy, 2016).

While virtually all of the recent literature has focussed on low pressure-based transport (at 7 bar and -50°C) (Geske et al., 2015; Knoope et al., 2015b; Roussanaly et al., 2013b), the question of optimal transport conditions (pressure, temperature and composition) is being raised as CCS chains based on ship transport are moving closer to implementation (Ministry of Petroleum and Energy, 2016). Indeed, the ship option that is often pushed forward in these chains involves transport at 15 bar and -30°C, as experience with liquefaction and transport under these conditions exists from the transport of food-grade CO_2 (IEAGHG, 2017). However, these conditions may not be optimal for transport of CO_2 in the case of CCS, and to date, no study has come to a conclusion regarding optimal ship transport conditions for CCS. For example, Seo et al. (Seo et al., 2016) pointed out that transport conditions above 25 bar do not appear to be cost-effective, although their results were inconclusive for the pressure range of key interest (7-20 bar). Furthermore, the impact of impurities potentially present in the CO_2 stream after capture on the design and costs of the CO_2 liquefaction and transport process has scarcely been considered, although several studies (Brunsvold et al., 2016; Porter et al., 2016) on CO_2 conditioning and transport by pipeline have shown that it can be significant.

As a first step towards the identification of optimal transport conditions for ship-based CCS, this study focuses on the design and cost of CO_2 liquefaction prior to ship transport. In particular, the impact of the targeted transport pressure on the design and cost of the liquefaction process will be investigated for the case of a pure CO_2 stream after capture, as well as for cases in which the CO_2 delivered after CO_2 capture also contains impurities, in order to better understand the potential impact of impurities on optimal transport conditions.

The structure of this study is as follow. Firstly, the CO_2 liquefaction process as well as the technical and cost basis considered for evaluation are presented. Secondly, the impact of the targeted transport pressure on the design and cost of liquefaction is assessed for pure CO_2. Finally, the impacts of impurities potentially present in the CO_2 stream after capture are discussed.

This is the accepted version of an article published in International Journal of Refrigeration
DOI: 10.1016/j.ijrefrig.2019.04.011

2 Methodology

2.1 Study concept and case studies

This study investigates the impact of targeted liquid CO_2 delivery pressure on the design and cost of CO_2 liquefaction prior to ship-based transport for CCS application for CO_2 streams with different levels of purity. As illustrated in Figure 1, the system boundaries for this study start after CO_2 capture until the CO_2 is sent to buffer storage.

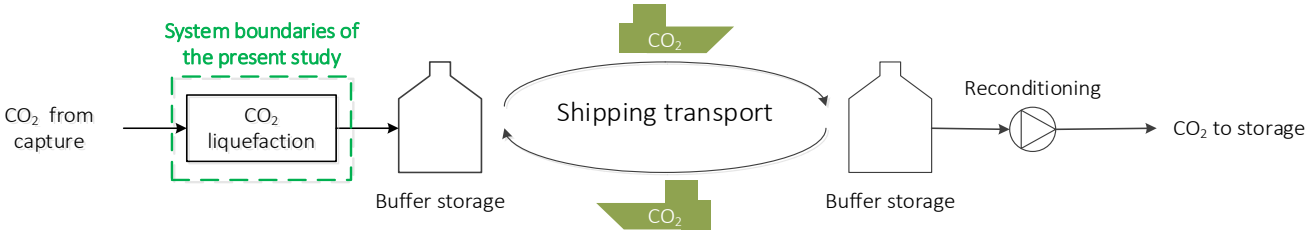

Figure 1: Overview of the ship-based CCS chain and system boundaries of the present studies

As illustrated in the phase diagram for pure CO_2 presented in Figure 2, CO_2 can be transported in liquid form at pressure from 5.2 to 73.9 bar. To identify the impact of targeted liquid CO_2 delivery pressure, the technical and cost performances of the CO_2 liquefaction process are assessed for 10 delivery pressures post-CO_2 liquefaction: 7, 10, 15, 20, 25, 30, 40, 50, 60, 70 bar. While these values were selected to be spread across the pressure range in which a liquid CO_2 phase exists, it is worth noting that the three first are often the most discussed. The 7 bar option, corresponding to the conditions similar to liquefied petroleum gas (LPG), is the one most commonly used in CCS literature (Decarre et al., 2010; Knoope et al., 2015a; Roussanaly et al., 2017). The 15 bar option corresponds to the transport condition currently used for transport of CO_2 in the food-grade industry (Ministry of Petroleum and Energy, 2016). Finally, the 10 bar option has recently been discussed as an intermediary option between the 7 and 15 bar system.

Even though high purity CO_2 (>95%) is normally obtained after capture, several studies have shown that the potential associated impurities can have a significant impact and cost of CO_2 conditioning and transport via pipeline (Porter et al., 2016; Skaugen et al., 2016). However, as limited data is available on the impact of impurity on the liquefaction of CO_2 prior to ship transport, this is here explored through different cases in term of impurities after capture impurity cases, as well as different constraints in term of purity after CO_2 liquefaction.

While the performances of the CO_2 liquefaction process are first assessed for a pure CO_2 stream, the impact of potential impurities in the CO_2 stream delivered by the CO_2 capture unit is also investigated through case studies. As the impurities present after capture depend on both the CO_2 source and the capture technology, many cases could be considered. Here, three impurity cases with different types and levels of impurities are selected based on previously documented studies: 1) Amine-based post-combustion CO_2 capture from a cement plant (Voldsund et al., 2019) 2) Membrane-based post-combustion CO_2 capture from a refinery (Roussanaly and Anantharaman, 2017) 3) Rectisol-based pre-combustion CO_2 capture from a coal power plant (Roussanaly et al., 2019). The composition of each of these cases is presented in Table 1.

Furthermore, for a given impurity case, the delivery pressures post-CO_2 liquefaction can have an impact on the purity of the delivered CO_2 after the liquefaction process. However, stronger purity constraints post-liquefaction may be imposed to the liquefaction process due to requirement down the chain (transport and or storage) Thus, the impact of purity requirement on the post-liquefaction CO_2 stream is also investigated through cases in which the delivered CO_2 is required to meet industrial-grade and food-grade purity requirements (≥99% and ≥99.9% purity respectively).

This is the accepted version of an article published in International Journal of Refrigeration
DOI: 10.1016/j.ijrefrig.2019.04.011

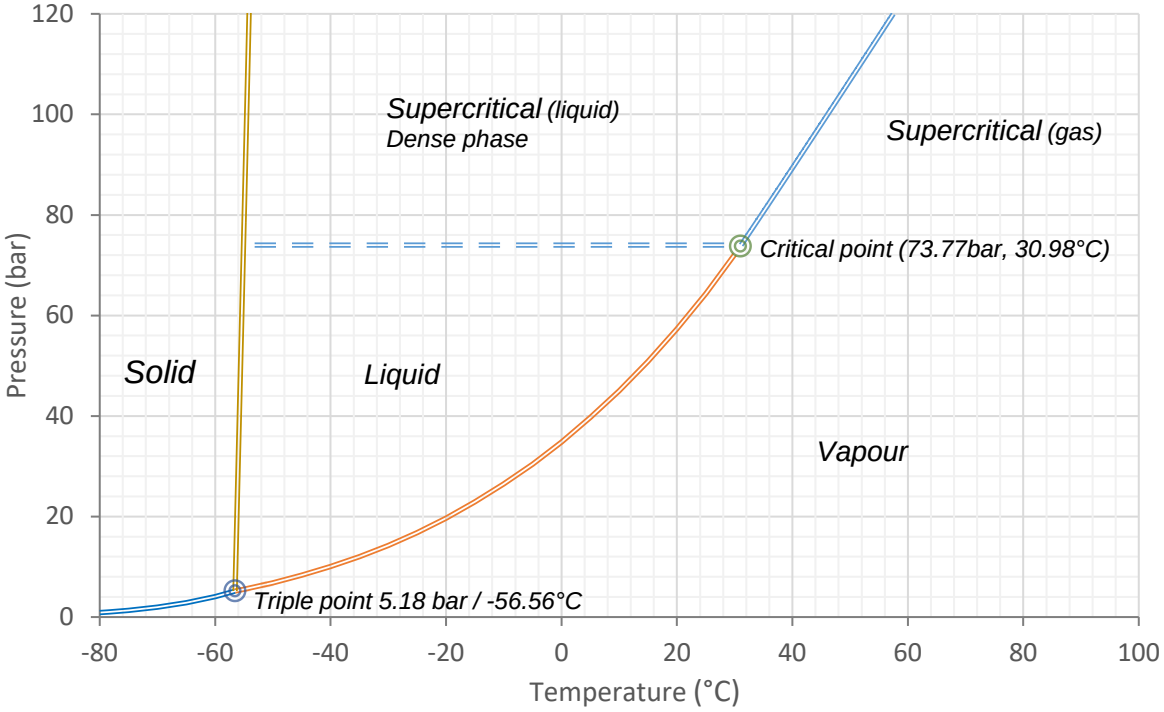

Figure 2: Phase diagram of pure CO_2 based on the Span and Wagner equation of state (Span and Wagner, 1996)

Table 1: Composition of the CO_2 stream in the impurity scenarios

Capture route	Post-combustion	Post-combustion	Pre-combustion
Capture technology	Amine	Membrane	Rectisol
CO_2 source	Cement plant	Refinery	IGCC
CO_2 [%]	96.86	97.0	98.42
H_2O [%]	3.00	1.0	
N_2 [%]	0.11	2.0	0.44
O_2 [%]	0.03		
Ar [%]	0.0003		0.09
MeOH [%]			0.57
H_2 [%]			0.45
CO [%]			0.03
H_2S [%]			0.0005
Total [%]	**100**	**100**	**100**

To ensure consistency between the different cases assessed, an integrated techno-economic optimisation model is used to design and evaluate the liquefaction process for both pure CO_2 (Section 3) and cases of CO_2 containing impurities (Section 4). The underlying technical and cost modelling of the optimisation model are presented in Sections 2.2 and 2.3.

Finally, to ensure that results are comparable, all cases consider a CO_2 stream with impurities entering the liquefaction process at a rate of 37.31 $kg.s^{-1}$ (equivalent to 1 $MtCO_2.y^{-1}$) (Lindqvist et al., 2014) available at 1 bar and 40°C (Voldsund et al., 2019). Although the flowrate of the CO_2 stream would depend on the CO_2 source considered, the CO_2 stream flowrate is expected to have a limited impact on the liquefaction cost as power related costs are the major cost drivers[1]. Lastly, although the CO_2 stream after capture may be available at different temperature and pressure conditions, the set pressure and temperature considered are selected to ensure comparability between the cases.

[1] However, it is worth noting that the scale effect will be included, in future work, when also taking into account the ship export due to the significant economies of scale of this part of the chain.

This is the accepted version of an article published in International Journal of Refrigeration
DOI: 10.1016/j.ijrefrig.2019.04.011

2.2 Technical modelling

The CO_2 liquefaction process modelling considered in this study is performed as an integrated techno-economic optimisation using non-linear programming by quadratic Lagrangian (NLPQL) (Schittkowski, 1986) as a general routine for solving a constrained non-linear optimisation problem. This implies that all the underlying models must be described as equality or inequality constraints with an objective function that should be minimised. In the present study, the optimisation aims to minimise the cost of the CO_2 liquefaction process. Thus, as Figure 3 shows, the optimisation model integrates process, component and cost models, which are further described below.

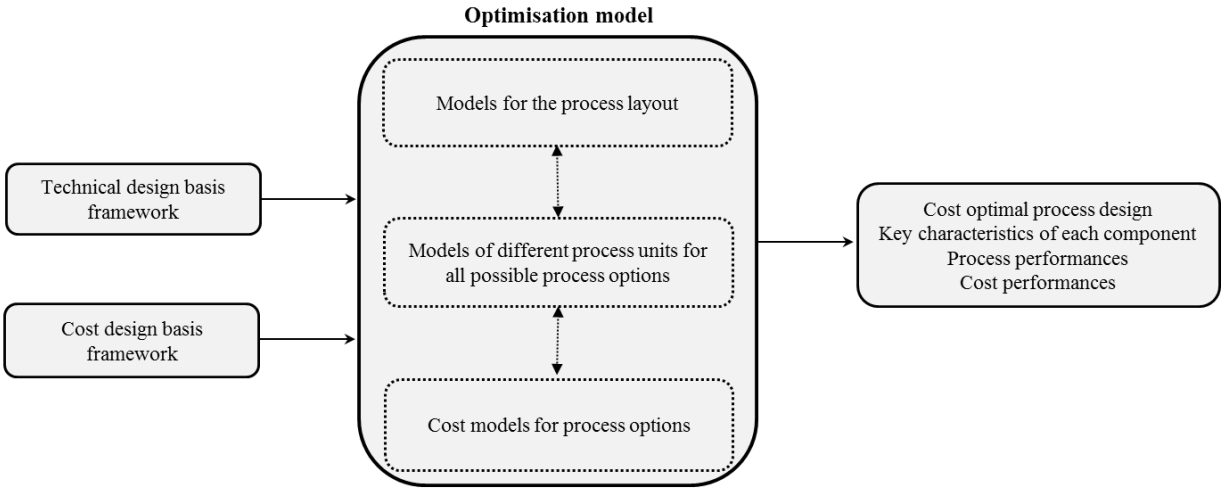

Figure 3: Structure of the optimisation model

2.2.1 Process layout

The liquefaction process layout adopted in the present study is shown in Figure 4. This process can be splitted in four sections: 1) the CO_2 compression train 2) the pre-cooler, liquefier and flash tank 3) Recirculation flash and compressor 4) the ammonia refrigeration cycle.

The CO_2 after capture, available at 1 bar and 40°C, enters the CO_2 compression train to undergo several stages of intercooled compression to achieve a pressure suitable for liquefaction at the outlet of ①. Depending on the desired liquefaction pressure, the compression can be either three or four stages[2]. Each compression stage consists of compression followed by intercooling and removal of condensed water through a flash separator.

Once the CO_2 stream has reached the desired liquefaction pressure, the CO_2 stream passes into an impurity removal unit ②, indicated as the square "box" in Figure 4, to remove potential impurities if required. The CO_2 stream is then cooled to 25°C in a pre-cooler ③, and further de-superheated and condensed in a liquefier based on an ammonia refrigeration cycle. After the liquefier ④, the CO_2 stream will end up being fully condensed and slightly sub-cooled in cases in which the CO_2 is pure or if the liquefaction pressure is high enough to also condense all impurities. For CO_2 streams that contain residual components, the bubble point temperature is much lower than for pure CO_2, and the CO_2 stream after the liquefier may only be partially condensed. In these cases, a flash tank ⑤ is used to purge the uncondensed gas, composed of impurities and some of the CO_2. This is necessary in order to prevent accumulation of impurities in the process. The liquid, that is mostly CO_2, passes through a valve ⑥ in order to reach the targeted delivery pressure level. The resulting stream passes through a separator ⑦ to separate the liquid CO_2, which is sent to buffer storage prior to ship transport, while the remaining gas is recirculated, after compression to the

[2] In the current setting, when liquefaction pressure is smaller than 25 bar, three compression stages are used, from the initial 1 bar to 3 bar (1st stage), to 9 bar (2nd stage), and to the final liquefaction pressure (last stage). If the liquefaction pressure is equal or higher than 25 bar, four stages of compression are used in a similar manner, where the stream is compressed from initial 1 bar to 27 bar with the first three stages and compressed to the desired liquefaction pressure in the final stage.

This is the accepted version of an article published in International Journal of Refrigeration
DOI: 10.1016/j.ijrefrig.2019.04.011

liquefaction pressure in a recirculation compressor ⑧, to be mixed with the main CO_2 stream before the pre-cooler ③.
It is worth noting that the refrigeration circuit "powering" liquefier is selected to be an ammonia-based two-stage vapour compression cycle with an intercooler ⑩ and a main heat exchanger (condenser) ⑫. The ammonia is only used as coolant in the liquefier ④, while all the other heat exchangers in the process are water-cooled, including the intercoolers of the compression train ①, the pre-cooler ③, as well as the intercooler ⑩ and the main heat exchanger ⑫ of the ammonia refrigeration cycle.
While the optimisation model considered is presented in Section 2.2.2, the component modelling adopted for each unit of the process is presented in Section 2.2.3.

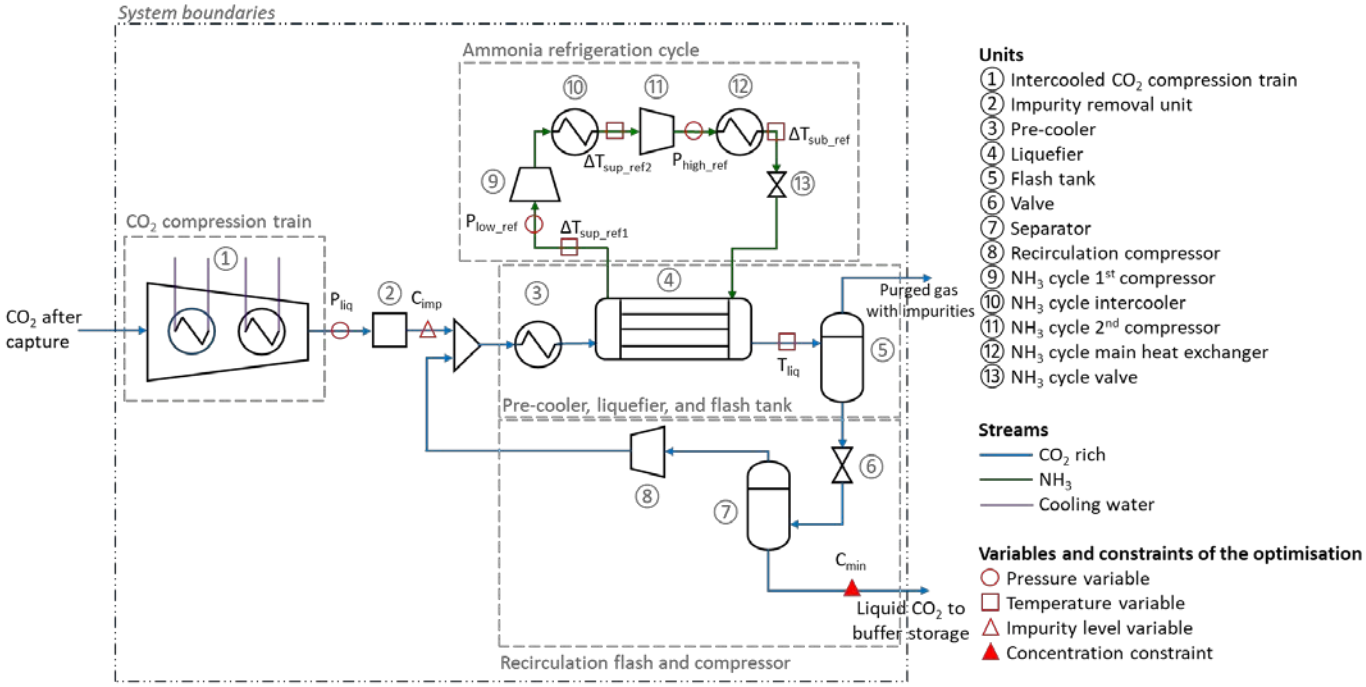

Figure 4: Process layout for the CO_2 liquefaction analysis

2.2.2 Optimisation model

As described in Section 2.1, the impact of post-liquefaction delivery pressure on the design and cost of CO_2 liquefaction will be studied for the scenarios (a) pure CO_2, (b) CO_2 with impurities, and (c) purity requirement of the delivered CO_2. The optimisation of the liquefaction process is solved by NLPQL (Schittkowski, 1986), which is an implementation of a sequential quadratic programming method. For the employment of NLPQL, the objective function, variables, and constraints must be set carefully. The objective function in the current model is defined as the CO_2 liquefaction cost (in €.tCO_2^{-1}) described in Section 2.3.3. While Figure 4 illustrates the variables and constraints, a detailed description for all the variables are listed in Table 2.
The pressure at the outlet of the final-stage compressor P_{liq}, namely the liquefaction pressure, is set as a variable. To ensure proper operation of the process, the lower boundary of P_{liq} is set to the delivery CO_2 pressure after the liquefaction process. Beyond the liquefaction pressure, the temperature of the CO_2 stream after the liquefier, T_{liq}, is also set as a variable of the optimisation model to allow a partial condensation or fully condensation in the liquefier ④. Indeed, for pure CO_2 cases, a subcooled CO_2 stream would be desired in order to prevent venting pure CO_2 through the gas purge of the flash tank ⑤. Meanwhile, for cases with impurities, partial condensation after the liquefier may be desired in order to purge impurities (non-soluble in the post-liquefaction CO_2) through the gaseous phase of the first flash tank in order to prevent their accumulation in the loop of the process.
In addition to the liquefaction pressure and temperature, the pressure and temperature levels of the ammonia refrigeration loop (pressure and temperature before the 1st compressor P_{low_ref} and ΔT_{sup_ref1}, temperature before the 2nd compressor ΔT_{sup_ref2}, pressure after the 2nd compressor P_{high_ref}, temperature after the ammonia cycle main heat exchanger ΔT_{sub_ref}) are also considered as variables of the process

This is the accepted version of an article published in International Journal of Refrigeration
DOI: 10.1016/j.ijrefrig.2019.04.011

optimisation as shown in Figure 4. These variables are taken into account in order to optimise the refrigeration process as part of the minimisation of the CO_2 liquefaction cost.
Finally, for cases in which the CO_2 entering the liquefaction process include impurities, both a purity variable and a purity constraint may be considered in the process optimisation. Indeed, for the cases with purity requirements, the impurities may need to be removed in order to meet the desired CO_2 purity after the liquefaction process. Although this impurity removal can be performed through the purge stream in the first flash of the process, this may result in significant CO_2 losses and an impurity removal may be more efficient in certain cases despite of potential high removal cost. In order to take this aspect into account, a "purity variable" (C_{imp}) is considered after the impurity removal unit in the model to optimise the composition of the CO_2 stream after the impurity removal unit. This "purity variable" thus set the type and level of impurity to be removed through the impurity removal unit in order to meet the post-liquefaction CO_2 purity (C_{min}).

Table 2: Variables considered in the optimisation of the CO_2 liquefaction process

Section	Variables	Description
CO_2 stream	P_{liq}	Pressure at outlet of intercooled CO_2 compression train ①
	T_{liq}	Temperature at outlet of liquefier ④
	C_{imp}	Impurity concentration after impurity removal unit ②
Refrigerant (NH_3) stream	P_{low_ref}	Pressure at inlet of refrigerant 1st compressor ⑨
	P_{high_ref}	Pressure at outlet of refrigerant 2nd compressor ⑪
	ΔT_{sup_ref1}	Superheated temperature at outlet of liquefier ④
	ΔT_{sup_ref2}	Superheated temperature at outlet of refrigerant cycle intercooler ⑩
	ΔT_{sub_ref}	Subcooled temperature at outlet of refrigerant cycle main heat exchanger ⑫

2.2.3 Component models

The liquefaction process shown in Figure 4 consists of the following process components: compressors, heat exchangers, impurity removal unit, mixing unit, valves, and separators. While the Peng-Robinson equation of state (Peng and Robinson, 1976) is used for the calculation of the thermodynamic properties and vapour-liquid equilibrium of CO_2 and CO_2 mixtures, the models adopted for each component are described below.

- **Compressors**

Compressors are modelled as an isentropic compression process corrected by an isentropic efficiency η_{is} of 85% (Anantharaman et al., 2011). With the given enthalpy at the compressor inlet h_{in} and the desired pressure at the compressor outlet, the outlet enthalpy by an isentropic process h_{is_out} can be obtained from the thermodynamic model. The outlet enthalpy h_{out} by a real compression process can be calculated as,

$$h_{out} = h_{in} + \frac{h_{is\_out} - h_{in}}{\eta_{is}} \qquad \text{(Eq. 1)}$$

The power consumption for each compression stage can thus be calculated as

$$W = \frac{\dot{m}(h_{out} - h_{in})}{\eta_{motor}} \qquad \text{(Eq. 2)}$$

where $\dot{m}$ is the mass flow rate, and η_{motor} is the motor efficiency, which is here set as 1.0.

- **Heat exchangers**

Heat exchangers are modelled based on counter-current units. To evaluate the design of a heat exchanger, the inlet and outlet characteristics of the two streams need to be specified. The cooling duty of the heat exchanger can be calculated based on the characteristics of the hot stream (CO_2 rich stream): mass flowrate, targeted temperature after cooling, and the specific heat capacity calculated based on the Peng-Robinson equation of state (Peng and Robinson, 1976). The mass flowrate of the cold stream (cooling water or ammonia depending on the heat exchanger considered) is then calculated by dividing the cooling

This is the accepted version of an article published in International Journal of Refrigeration
DOI: 10.1016/j.ijrefrig.2019.04.011

duty by the heat capacity (Ahrends and Baehr, 1979)[3] and the allowable temperature increase of the cold stream. Specifically, the CO_2 stream is always the hot side of the heat exchangers, while the cooling water or refrigerant is the cold side. It is worth noting that for the liquefier, the refrigerant mass flowrate is calculated as part of the optimisation procedure, as the refrigerant inlet and outlet conditions are free variables of the optimisation model.
The UA value (the product of the overall heat transfer coefficient and the heat transfer area) of the heat exchanger is then calculated based on the heat capacity and the log-mean temperature difference for counter current flow. With an overall heat transfer coefficient (U) assumed to be around 1000 $W.m^{-2}K^{-1}$ for all the process heat exchangers (Roussanaly et al., 2017), the heat exchange area (A) of each unit can then be assessed. While a heat exchanger model based on a detailed geometry could have also been used, this simplified model is here selected as a trade-off between detailed modelling and computation time in order to estimate the heat exchanger cost.

- **Separators**

The flash separator model includes one stream at the inlet, and one liquid stream and one gas stream as the outlets. The two outlets are simply obtained as the liquid and gas phases of the inlet stream.
The volume of each flash separator is calculated assuming a vertical tank with a residence time of 5 min and assuming that the liquid volume represents 50% of the total separator volume (Branan, 2005).

- **Mixers**

The mixing units are used to mix the main CO_2 stream with the recirculated stream. The inlet streams of the mixing units are at the same pressure but have different temperatures. The mass and concentration of the mixed stream at the outlet are calculated based on the mass conservation of each component in inlet streams. The specific enthalpy at the outlet is computed by a weighted average of each inlet stream *i* as,

$$h = \frac{\sum h_i \dot{m}_i}{\sum \dot{m}_i} \qquad \text{(Eq. 3)}$$

The temperature and thermodynamics properties are then obtained from the thermodynamic model based on the concentration, specific enthalpy, and pressure of the mixed stream.

- **Valves**

Valves are modelled as an isenthalpic expansion. As a result, the characteristics of the outlet stream can be calculated from the thermodynamic model knowing the outlet pressure.

- **Impurity removal unit**

An impurity removal unit is also included prior to the CO_2 cycle in order to dehydrate the CO_2 to prevent freeze-out in the process and remove other impurities present in the CO_2 when purging of impurities is not sufficient to meet the purity constraint on the post-liquefaction CO_2. While the amount and type of impurities are selected as part of the global process optimisation model, the impurity removal unit is modelled based on a "simple" mass balance.

2.3 Cost assessment methodology

A bottom-up approach, described below, is here considered to evaluate the cost of the CO_2 liquefaction process. It is worth noting that all estimates presented are given in 2015 Euro prices.

2.3.1 Investment cost

In this bottom-up approach, the direct costs of the different components of the process are based on cost functions. These cost functions were regressed, for each piece of equipment considered, based on multiple evaluations performed with Aspen Process Economic Analyzer® as documented in Appendix A. To ensure the validity of these functions for the conditions encountered in the optimisation model, a wide range of key component characteristics were carefully selected for each piece of equipment considered. Based on these component-specific cost functions, the direct cost (DC) of each component of the liquefaction process is assessed, in the appropriate material, using the corresponding key characteristics obtained

[3] The specific heat capacity of ammonia is calculated based on the Ahrends and Baehr equation of state.

This is the accepted version of an article published in International Journal of Refrigeration
DOI: 10.1016/j.ijrefrig.2019.04.011

through the technical modelling process. Process contingencies of 15% (NETL, 2011) are then added to the total direct cost. Finally, to reach the total plant cost, the total direct cost with process contingencies is multiplied by 1.41 to include indirect costs (14%), owner costs (7%) (Anantharaman et al., 2011), and project contingencies (20%) (NETL, 2011).
Figure 5 illustrates the bottom-up evaluation of total plant cost (TPC) of the liquefaction process.

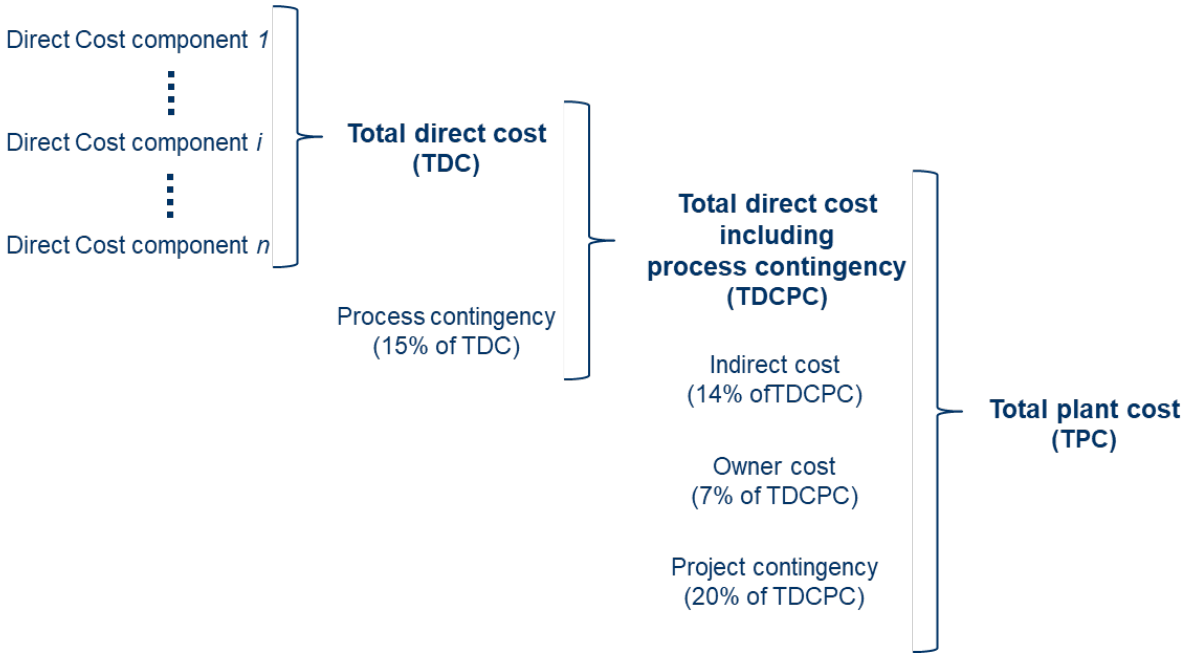

Figure 5: Illustration of the methodology to assess the Total Plant Cost of the liquefaction process

2.3.2 Operating costs

The CO_2 conditioning process results in both fixed operating costs, independent of the utilisation rate of the facility, and variable operating costs. The annual fixed operating costs include maintenance, insurance and labour costs and replacement of materials, and are set to 6% of the total plant cost (Roussanaly et al., 2017).
The variable operating costs cover consumption of utilities, such as electricity and cooling water, as well as a penalty cost for potential CO_2 losses through the purge stream. The annual cost for utilities is based on estimated consumption of utilities and the utility cost reported in Table 3. Similarly, the cost associated with losses of CO_2 through the purge is based on estimated CO_2 purge flow and a penalty cost for CO_2 losses. Here, the penalty cost is assumed to be 50 €.t_{CO2}^{-1} (Anantharaman et al., 2011),to represent the cost spent capturing the CO_2 which ends up being lost through the purge.

Table 3: Cost of utilities

Utility	Cost
Electricity [€.$MW^{-1}h^{-1}$]	80 (IEAGHG, 2013)
Cooling water [€.m^{-3}]	0.025 (Husebye et al., 2012)

2.3.3 CO_2 liquefaction cost

The CO_2 conditioning cost (€.t_{CO2}^{-1}) is here considered as a key performance indicator, in order to optimise and represent the cost of the CO_2 conditioning process. As illustrated in Eq. 4, the CO_2 conditioning cost is calculated by dividing the annualised costs of the process divided by the annual amount of CO_2 sent for ship transport (Skaugen et al., 2016). Finally, it is worth noting that the CO_2 conditioning cost is calculated based on a discount rate of 8%, an economic lifetime of 25 years, and that the conditioning facility is built over a three-year period (with a 40/30/30 annual allocation) (Anantharaman et al., 2011).

$$\text{CO}_2 \text{ conditioning cost } (€.t_{CO2}^{-1}) = \frac{\text{Annualised investment + Annual operating cost}}{\text{Annual amount of CO}_2 \text{ sent for transport}} \quad \text{(Eq. 4)}$$

This is the accepted version of an article published in International Journal of Refrigeration
DOI: 10.1016/j.ijrefrig.2019.04.011

3 Results for pure CO_2

The following sections illustrate the impact of the delivery CO_2 pressure post-liquefaction on the liquefaction process design (Section 3.1) and its cost performances (Section 3.2) in the case of conditioning of a pure CO_2 stream.

3.1 Impact of delivery CO_2 pressure post-liquefaction on the design of the liquefaction case of a pure CO_2 stream

The design and cost of CO_2 liquefaction have been assessed for 10 delivery pressures post-liquefaction for the case of pure CO_2.

The power consumption and cooling duty for the liquefaction of pure CO_2 under the different delivery pressures are shown in Figure 6 and Figure 7, respectively. Table 4 provides a detailed breakdown of the power consumption and cooling duty together with some important design parameters. It can be seen from Figure 6 that the total compression power reaches minimum values at delivery pressures of 30 to 50 bar. As the targeted delivery pressure rises, the power requirement of the CO_2 compression train increases, while the compression power of the compressors of the ammonia cycle and the power of the recirculation compressor are reduced. Meanwhile, the total cooling duty is almost halved when the delivery pressure increases from 7 bar to 70 bar. Specifically, the cooling requirement associated with each heat exchanger of the CO_2 compression train and the liquefier is only slightly decreased, while the cooling of the liquefier and the cooler of the ammonia cycle decreases significantly.

The total compression power is composed of the power of the CO_2 compression train, the compressors of the ammonia cycle, and the recirculation compressor. The three parts of compression power interact under different liquefaction pressure and delivery pressures. The impact of liquefaction pressure (i.e. liquefier pressure) on the power consumption is illustrated in Figure 8, with an example of delivery pressure at 7 bar. When the CO_2 stream is compressed at a higher liquefaction pressure, the compression train power increases, as does the liquefaction temperature. The results of the evaluation indicate that the temperature difference between the hot and cold stream in the liquefier will always approach the permitted minimum value in order to minimise power consumption. Thus, a higher liquefaction temperature will allow a higher refrigerant temperature, which results in lower power consumption of the ammonia cycle. However, a larger pressure difference between the liquefaction pressure and delivery pressure will give a greater mass flow of the recirculated CO_2 stream, which means that a higher liquefaction pressure at a given delivery pressure will increase the compression power needed for recirculating the stream. It can be seen from Figure 8 that the minimum power consumption for a delivery pressure of 7 bar is at a liquefaction pressure around 20 bar.

As pure CO_2 is fully condensed in the liquefier, no purge is required for any of the delivery pressures. Thus, as can be seen in Table 4, all the CO_2 entering the liquefaction process (37.31 $kg.s^{-1}$) is delivered as liquid CO_2 without losses through the purge.

As delivery pressure increases, the CO_2 is compressed to a higher liquefaction pressure P_{liq}. However, it is worth noting that for delivery pressure above 25 bar, the optimal the liquefaction pressure P_{liq} is always slightly higher than the targeted delivery pressure. Indeed, the smaller difference between the liquefaction pressure and delivery pressure is part of the reason for the decrease of the power consumption for re-compression.

As the target delivery pressure increases, the temperature of the delivered CO_2 increases and the CO_2 density decreases, which means that a larger tank will be required to transport the same quantity of CO_2.

This is the accepted version of an article published in International Journal of Refrigeration
DOI: 10.1016/j.ijrefrig.2019.04.011

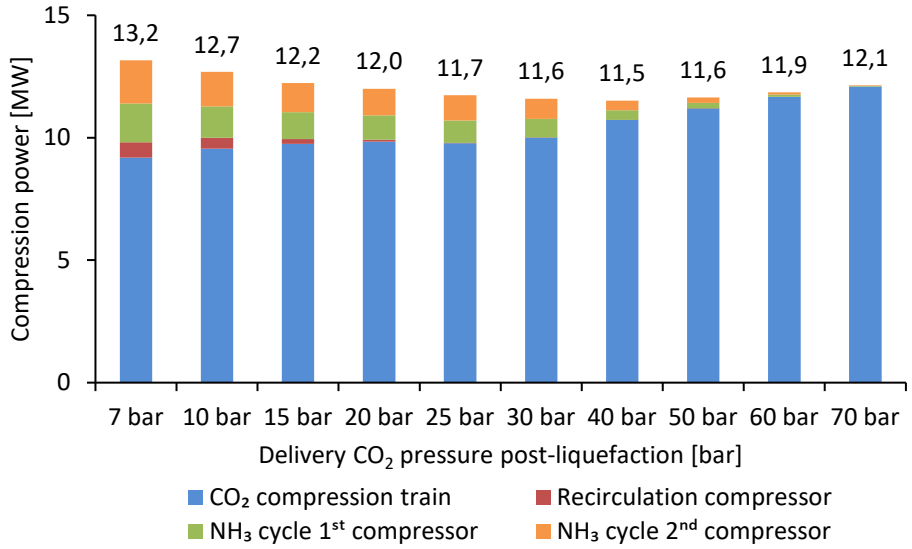

Figure 6: Power consumption for the liquefaction of pure CO_2

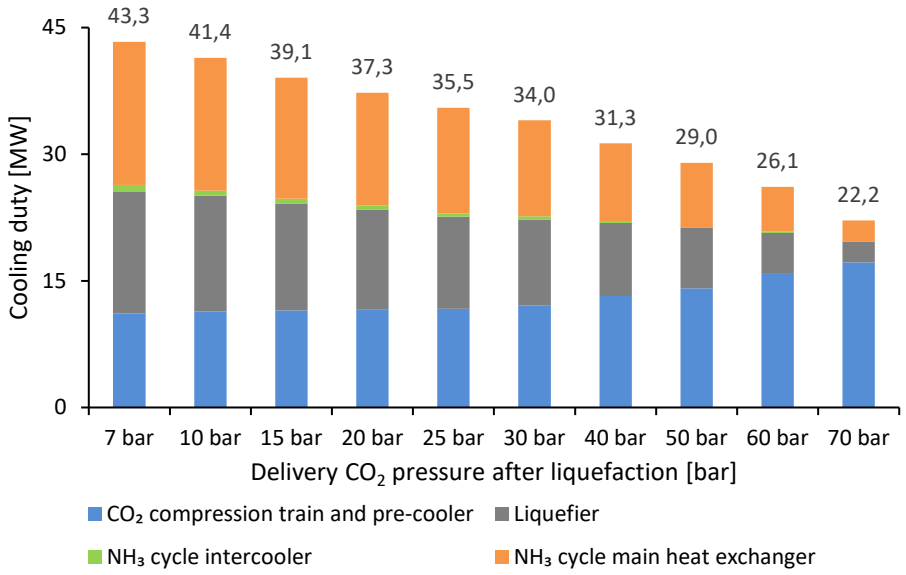

Figure 7: Cooling duty for the liquefaction of pure CO_2

This is the accepted version of an article published in International Journal of Refrigeration
DOI: 10.1016/j.ijrefrig.2019.04.011

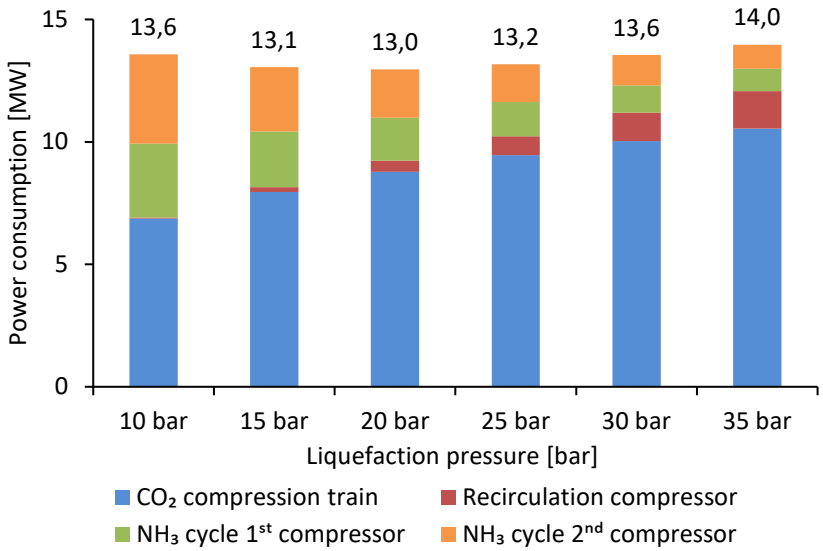

Figure 8: Power consumption with various liquefaction pressures under a delivery pressure of 7 bar

Table 4: System performance under different delivery pressures

Pressure	7	10	15	20	25	30	40	50	60	70
Compression power [MW]	13.17	12.68	12.24	12.00	11.73	11.59	11.50	11.65	11.85	12.14
CO_2 compression train	9.19	9.55	9.75	9.85	9.78	10.01	10.67	11.21	11.67	12.09
Recirculation compressor	0.64	0.45	0.20	0.07	0.01	0.00	0.00	0.00	0.00	0.00
NH_3 cycle 1st compressor	1.58	1.27	1.09	1.00	0.92	0.76	0.41	0.21	0.08	0.03
NH_3 cycle 2nd compressor	1.76	1.41	1.19	1.09	1.03	0.82	0.42	0.23	0.09	0.03
Cooling duty [MW]	43.30	41.42	39.08	37.30	35.50	34.01	31.31	28.99	26.14	22.17
CO_2 compression train	7.37	7.37	7.37	7.37	11.20	11.20	11.20	11.20	11.20	11.20
Precooler	3.77	4.03	4.13	4.20	0.50	0.91	2.01	2.92	4.60	5.98
Liquefier	14.41	13.67	12.64	11.82	10.92	10.15	8.64	7.21	4.88	2.46
NH_3 cycle intercooler	0.82	0.61	0.57	0.53	0.37	0.37	0.25	0.01	0.19	0.02
NH_3 cycle main heat exchanger	16.93	15.74	14.36	13.37	12.51	11.37	9.22	7.65	5.25	2.50
P_{liq} [bar]	22.9	25.8	27.5	28.3	28.0	31.0	41.0	51.0	61.0	71.0
Recirculated mass flowrate [$kg.s^{-1}$]	2.03	0.58	0.48	0.44	1.34	0.42	0.99	0.05	0	0
Stored liquid T [°C]	-49.1	-39.8	-28.2	-19.2	-11.7	-5.3	5.4	14.3	21.9	28.7
Stored liquid density [$kg.m^{-3}$]	1133	1095	1042	995.4	952.2	910.9	830.3	747.6	655.8	531.2
Stored liquid mass flowrate [$kg.s^{-1}$]	37.31	37.31	37.31	37.31	37.31	37.31	37.31	37.31	37.31	37.31

3.2 Impact of delivery CO_2 pressure post-liquefaction on the cost performances of the liquefaction of a pure CO_2 stream

Figure 9 presents the total direct cost (TDC) of the CO_2 liquefaction process, as a function of the delivery CO_2 pressure after liquefaction, with a breakdown between the four sections of the concept: 1) CO_2 compression train 2) Pre-cooler, liquefier and flash tank 3) Recirculation flash and compressor 4) Ammonia refrigeration cycle.

The evaluations show that the total plant cost ranges from 25.5 M€ for a 7 bar delivery pressure to 23.6 M€ for a delivery pressure of 60 bar. As illustrated by the TDC breakdown, there is a limited reduction in

This is the accepted version of an article published in International Journal of Refrigeration
DOI: 10.1016/j.ijrefrig.2019.04.011

TDC as delivery CO_2 pressure increases, which can be explained principally by two important trends. First, the TDC associated with the ammonia refrigeration cycle decreases by 70% as the delivery pressure increases, due to the reduced cooling requirement as the liquefaction pressure increases. Secondly, the TDC linked with the compression train increases only to a limited extent (15%) as the delivery pressure increases from 7 to 70 bar. Indeed, despite the greater increase in the power of the compression train, the associated TDC increases only to a certain extent as the compression stages at high pressures are cheaper than at low pressures in term of €.kW^{-1}.
As a consequence of these variations, the TDC breakdown changes significantly as the delivery pressure increases. For example, at 7 bar, the compression train and the ammonia refrigeration cycle represent respectively 54 and 30% of the TDC, while the compression train alone accounts for 67% of TDC at 70 bar.
Finally, it is worth noting that although the TDC decrease slightly as the pressure increase, a small increase in TDC can be observed at 25 bar as, beyond this pressure, the CO_2 compression train takes four stages to reach the optimal liquefaction pressure.

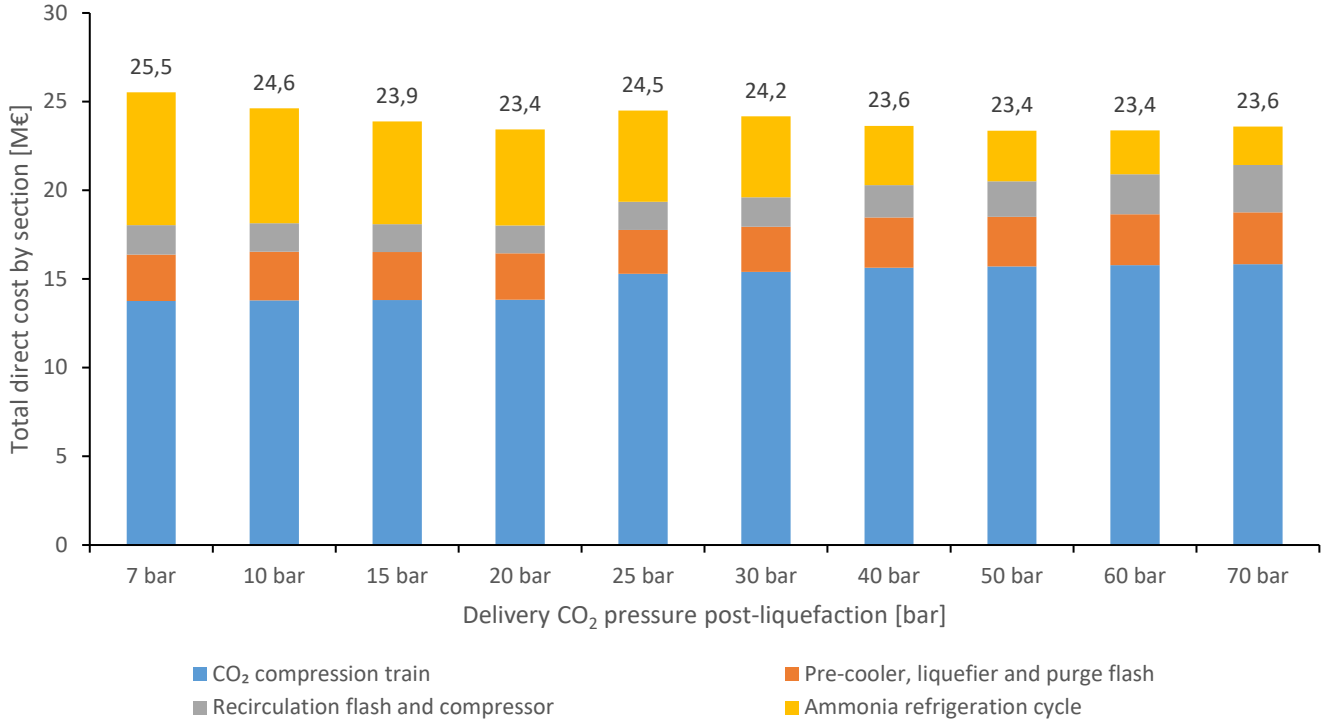

Figure 9: Total Direct Cost in function of the delivery CO_2 pressure post-liquefaction in the case of pure CO_2

Based on the process design selected and the cost evaluation methodology, the CO_2 liquefaction cost of a pure CO_2 stream was assessed for the considered range of delivery pressures after the liquefaction process, as shown in Figure 10. Overall, the cost evaluations show that the CO_2 liquefaction cost ranges from 13.4 to 15.2 €.tCO_2^{-1}, depending on the delivery pressure after liquefaction. For all cases, the cost breakdown emphasises that electricity consumption is the main contributor to total costs (around 50%), while investment costs and fixed operating costs represent around 28% and 17% respectively of the CO_2 liquefaction cost.
The evaluation shows that the delivery pressure resulting in the highest CO_2 liquefaction cost is the 7 bar option, which results in a cost of 15.2 €.tCO_2^{-1}. As the delivery pressure increases, the CO_2 liquefaction cost falls until reaching a minimum cost 13.4 €.tCO_2^{-1} around 50 bar, thus achieving a cost reduction of 12% compared to the 7 bar case. However, it is worth noting that most of the decrease takes place between 7 and 20 bar as the CO_2 liquefaction cost is reduced by 9% between these two cases. In both cases, the decrease is due to both the reduction in power consumption associated with the process and the lower investment costs. Meanwhile, beyond 50 bar, a small increase in CO_2 liquefaction cost is observed due to

This is the accepted version of an article published in International Journal of Refrigeration
DOI: 10.1016/j.ijrefrig.2019.04.011

the slight increase in power requirements beyond this point. These results appear to follow the same trend as those illustrated by Seo et al. [23].
Finally, as these cases are currently the most discussed for ship-based CCS implementation, it is interesting to also directly compare the 7 and 15 bar cases. The case evaluation demonstrates that the 15 bar case results in a CO_2 liquefaction cost that is almost 7% lower than the 7 bar case (i.e. 1.05 €.tCO_2^{-1} cheaper). However, it is important to remember that the presence of the potential impurity in the CO_2 stream and purity requirements can have an impact on this comparison, and that the entire transport chain must be considered to identify the optimal pressure at the interface between liquefaction and ship-based transport.

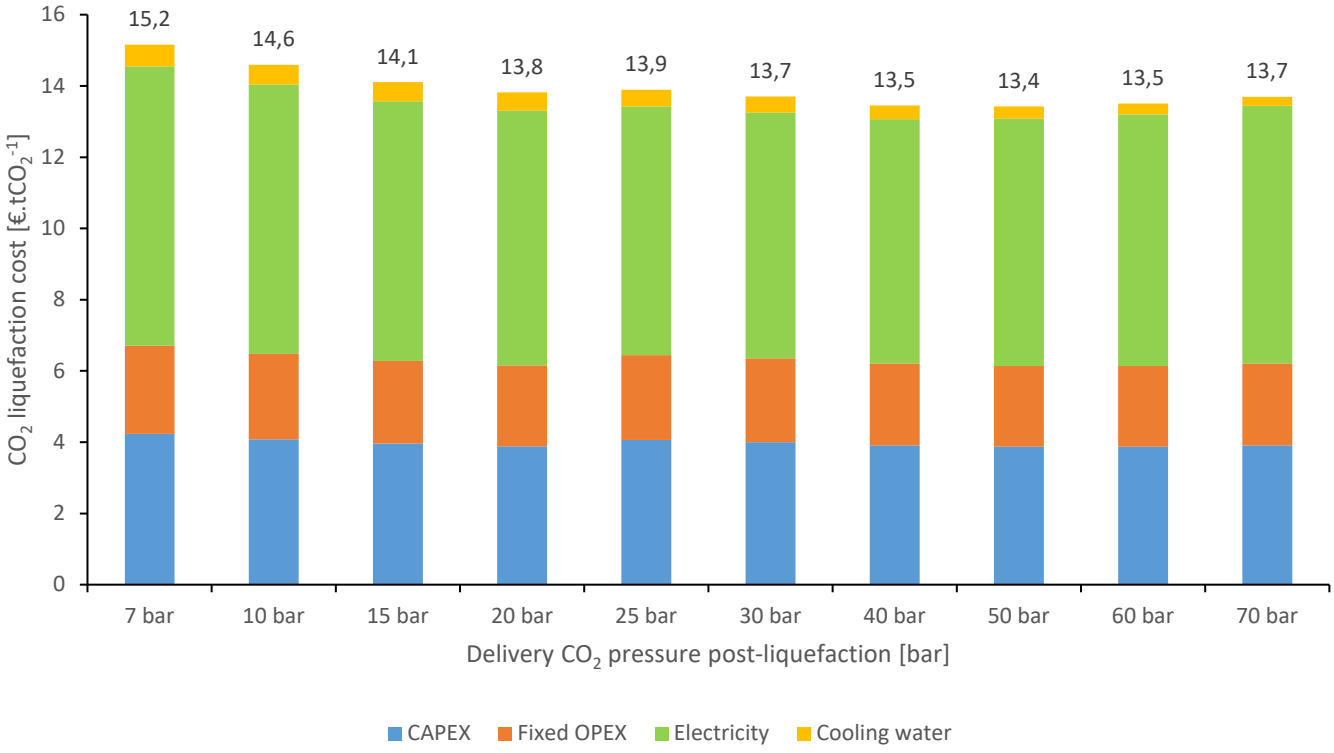

Figure 10: CO_2 liquefaction cost for different delivery CO_2 pressures post-liquefaction for pure CO_2

4 Results for CO_2 containing impurities

In this section, the impact of both potential impurities present in the inlet CO_2 stream and potential purity requirements on the CO_2 delivered by the liquefaction process on the CO_2 liquefaction process is discussed through the three impurity scenarios presented in Table 1.

4.1 Impact of potential impurities present in the CO_2 stream if no purity requirement on the CO_2 post-liquefaction is considered

In this section, it is worth noting that no requirement is imposed on CO_2 purity after the liquefaction process. However, as the potential impurities may not be fully soluble in the CO_2 stream after liquefaction, these impurities must be vented through the flash tank of the process in order to prevent their accumulation in the loop of the process. As a result of this impurities purge, some CO_2 may also be vented depending on the flash tank operating conditions. Thus, a minimum recovery of 95% of the CO_2 entering the liquefaction process is imposed in order to avoid designs resulting in high CO_2 losses associated with the purging of non-condensable impurities.

This is the accepted version of an article published in International Journal of Refrigeration
DOI: 10.1016/j.ijrefrig.2019.04.011

While the technical process characteristics and cost breakdown obtained from the process optimisation are presented in Appendix B.2, the CO_2 liquefaction costs obtained for the different CO_2 impurity scenarios from Table 1 are plotted in Figure 11 as functions of the delivery CO_2 pressure. The results emphasise that potential impurities present in the CO_2 stream after capture can lead to significant increases in CO_2 liquefaction costs compared to pure CO_2 (up to 34% for the cases considered here). Overall, delivery pressures below 30 bar seems to be the most heavily impacted by the different impurity cases, while a more moderate increase is observed beyond. However, it is also important to note that this increase is also specific to the impurity case considered. The membrane-based case seems to be the most affected (+3-34%), followed by the Rectisol-based case (+0-14%), and finally the amine-based case (+2-11%). These differences between cases underline the fact that both the type and level of impurities have a significant impact. Indeed, although the amine- and membrane-based cases have the same level of impurities (around 3%), very different responses are observed as most of the impurities in the amine case is water which has less impact on the liquefaction process as it is condensed during the compression train and dried before the ammonia refrigeration cycle. Furthermore, although the membrane- and rectisol-based cases have similar levels of non-aqueous impurities (2% v.s. 1.6%), the membrane case is significantly more affected, as most of these impurities are more difficult to separate. When looking at the cost breakdown presented in Appendix B.2, the rise in costs in cases with impurities appear to be linked both to the higher cost of the liquefaction process, due to higher compression and cooling requirement, and to the CO_2 losses through the purge, which result in a penalty cost and a reduction in the amount of CO_2 delivered by the liquefaction process.

Beyond the increase in cost resulting from the impurity scenario, these results also help to understand how impurities could impact the comparison between delivery CO_2 pressure post-liquefaction and thus the optimal transport pressure for ship-based transport. Indeed, while the liquefaction process delivering CO_2 at 15 bar is 1.05 €.tCO_2^{-1} cheaper than at 7 bar for pure CO_2, this difference varies between the impurity cases. While the difference is slightly higher in the Rectisol case (1.3 €.tCO_2^{-1}), the amine and membrane cases result in greater differences (1.7 € and 1.6 €.tCO_2^{-1} respectively), and could thus affect the selection of the optimal transport solution. However, as potential impurities have a lower impact on the liquefaction cost at high pressure, these potential impurities thus affect less the comparison between delivery CO_2 pressures post-liquefaction beyond 30-40 bar.

Finally, it is important to note that no constraint in CO_2 purity requirement was here considered and that considering such a constraint could further influence the selection of the optimal transport condition, especially as the purity of the CO_2 delivered by the liquefaction process is reduced as the delivery pressure increases.

This is the accepted version of an article published in International Journal of Refrigeration
DOI: 10.1016/j.ijrefrig.2019.04.011

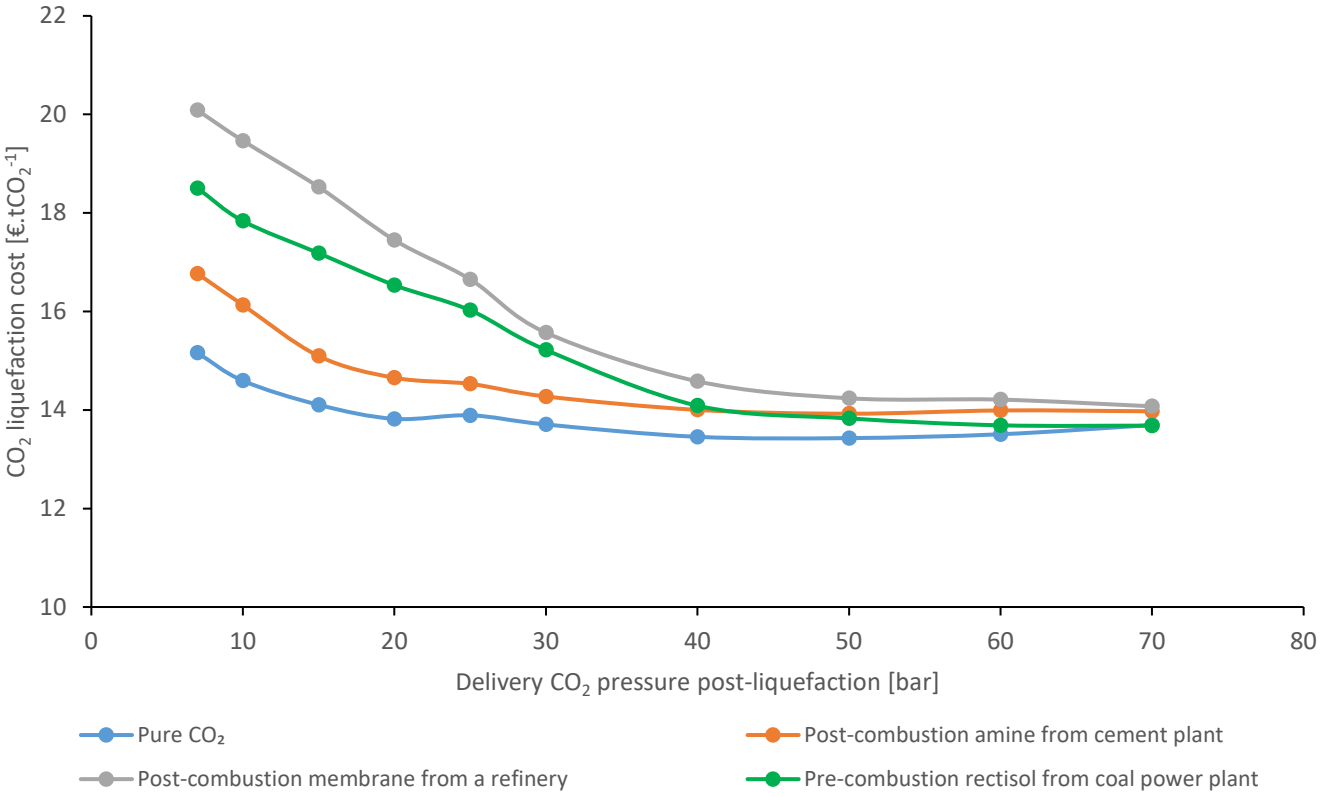

Figure 11: CO_2 liquefaction cost for different delivery CO_2 pressures post-liquefaction in the different CO_2 purity cases

4.2 Impact of potential impurities present in the CO_2 stream if a purity requirement on the CO_2 post-liquefaction is considered

Although not considered in section 4.1, purity constraints on the CO_2 delivered by the liquefaction process may be imposed due to requirement downstream of the liquefaction process, for example, imposed by the ship transport or the CO_2 storage. The impact of this potential requirement on the cost of the CO_2 liquefaction process is here explored for the impurity scenario corresponding to the post-combustion membrane from a refinery case. Two sets of purity constraints are here considered: 99% (high purity CO_2) and 99.9% (food-grade CO_2 purity). To meet the purity, the optimisation model designs the process to remove the impurities through purging when possible or also through an impurity removal unit, located after the final compression stage, when purging is not sufficient[4]. In cases in which impurities must be removed through an impurity removal unit, the model also selects the type and quantity of impurities to be removed as part of the optimisation of the CO_2 liquefaction process taking into account a penalty cost for the removal of these impurities[5]. Finally, as in the Section 4.1, a minimum recovery of 95% of the CO_2 entering the liquefaction process is imposed in order to avoid designs resulting in high CO_2 losses associated with the purging of non-condensable impurities.

The CO_2 liquefaction cost for different delivery CO_2 pressures is presented in Figure 12 and Figure 13 for 99% and 99.9% purity constraints respectively. The results previously obtained for pure CO_2 and when no purity constraint is considered, here used as references, are presented in plain line. The results when a purity constraint is considered are presented in coloured square markers: when considering only purge (green) and when also using an impurity removal unit with a removal cost of 300 €/t (yellow), 400 €/t (purple), and 500 €/t (red).

[4] As the impurity removal unit is expected to be more costly than the impurity removal through the purge.

[5] In practice, the impurity removal cost is highly dependent on the type and level of impurities to be removed. Due to both this specificity and the lack publicly available data, a range of impurity costs of 300-500 €/$t_{impurities}$ tough to be representative of such costs is here considered.

This is the accepted version of an article published in International Journal of Refrigeration
DOI: 10.1016/j.ijrefrig.2019.04.011

In the 99% purity constraint case, the results show that the purity constraint does not result in additional costs below 15 bar, since the CO_2 delivered by the liquefaction process already satisfies the purity requirement. At 20 and 25 bar, additional purging is needed to meet the purity requirement. However, for pressure above 30 bar, purging is not enough to meet the purity requirement and impurity removal after compression must be considered. These process modifications required beyond 20 bar result in additional costs. As a consequence, the cost difference between the 7 and 70 bar pressure cases is significantly reduced when impurity should be removed. While this difference represented 6 €.tCO_2^{-1} in the case without a purity constraint, this difference in the 99% purity constraint case ranges between 3.2 and 4.5 €.tCO_2^{-1}, depending on the cost of impurity removal. This reduces the cost advantage of the high delivery pressure post-liquefaction in the 99% purity case.

In the 99.9% purity constraint case, the cost of CO_2 liquefaction leads to different trends as the high purity constraint requires impurity removal for all the delivery pressures considered. As a consequence, the cost difference between the 7 and 70 bar cases becomes 3.2 €.tCO_2^{-1}, independently of the impurity removal cost, thus halving the cost difference compared to when no purity constraint is involved.

It is worth noting that the purity constraints do not affect the difference in cost between the 7 and 15 bar delivery pressures, for the impurity scenario considered compared to when there is no purity constraint, as the purity constraint is already met in the 99% case and impurity removal is required for both delivery pressures in the 99.9% case. Although this is not the case here, the combination of impurities present in the CO_2 stream and the purity requirement could have a significant impact on the comparison: 1) if only the 15 bar pressure requires additional purification to meet the purity constraint 2) or if either of the pressure need dedicated further removal of specific impurities. However, this can only be evaluated on a case-to-case basis.

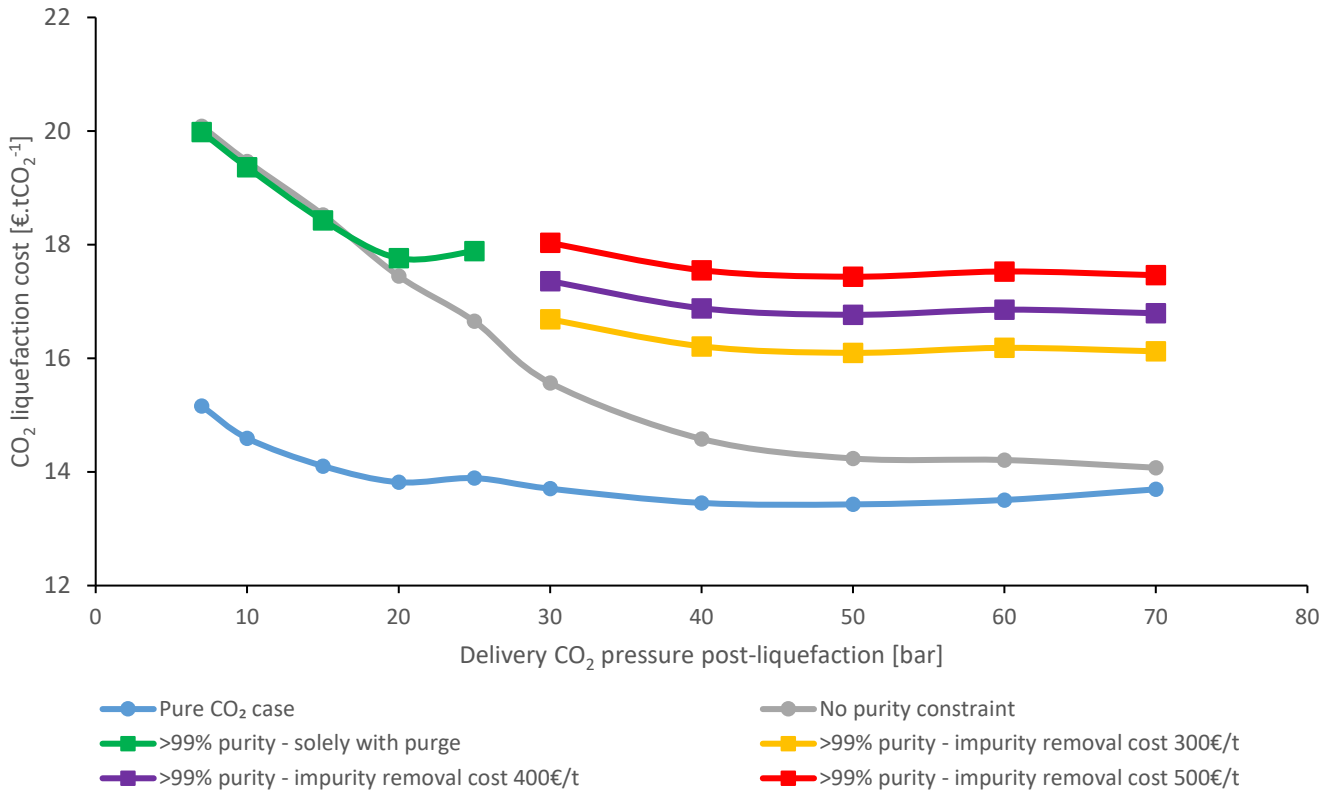

Figure 12: CO_2 liquefaction cost for different delivery CO_2 pressures, for pure CO_2, no purity constraint and 99% purity constraint in the case of post-combustion membrane-based capture from a refinery

This is the accepted version of an article published in International Journal of Refrigeration
DOI: 10.1016/j.ijrefrig.2019.04.011

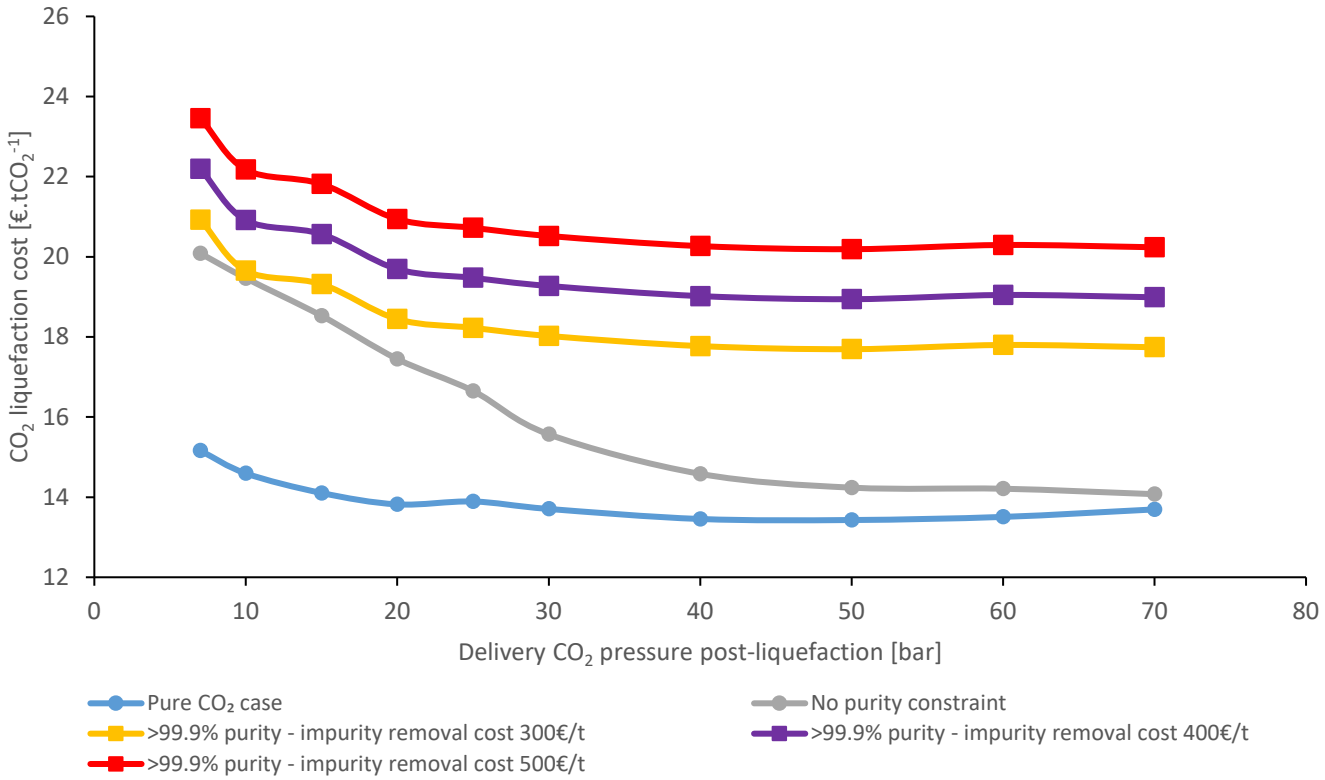

Figure 13: CO_2 liquefaction cost for different delivery CO_2 pressures, for pure CO_2, no purity constraint and 99.9% purity constraint in the case of post-combustion membrane-based capture from a refinery

5 Conclusions

While pipeline transport has traditionally been treated as the best option for transporting CO_2 due to its low cost for short distances and the important economies of scale involved, the momentum for ship-based transport of CO_2 is rising due to its cost-effectiveness for long distances and small volumes, low capital requirements, flexibility, short construction time and opportunities for co-utilisation of infrastructure. Over the past few years, the question of optimal transport conditions (pressure, temperature and purity) for ship-based transport of CO_2 has arisen due to the difference between the conditions considered in most of the literature (~7 bar) and industrial experience from the food industry (~15 bar). As a first step towards the identification of the optimal transport conditions for CO_2 shipping, this study investigates the impact of the delivery pressure post-liquefaction on the design and cost of the liquefaction process for (a) pure CO_2 (b) various impurity scenarios (c) different purity requirement constraints.

For pure CO_2, the highest liquefaction cost occurs at 7 bar, while a minimum is obtained around 40-50 bar (13% cheaper than at 7 bar) due to the significant reduction in the power requirement associated with cooling of the CO_2 stream. In the comparison of the 7 and 15 bar options, this led to a cost reduction of 1.05 €.tCO_2^{-1} in the 15 bar case. Under different potential impurity scenarios, the difference between the low and high pressures increase significantly as impurities need to be purged for the low-pressure cases as they are not soluble in the CO_2 stream delivered after the liquefaction process. This raises the liquefaction cost by up to 34% compared to the pure CO_2 case and increases the differences between the pressure levels, particularly for pressures below 30 bar. It also affects the comparison between the reduction in cost at 15 bar delivery pressure compared to 7 bar, which varies between 1.3 and 1.7 €.tCO_2^{-1} depending of the impurity scenarios considered. Furthermore, potential purity requirements also prove to have a significant impact on comparisons of the delivery pressure, although this impact is dependent on both the impurities present and the purity requirement considered.

Finally, although the results presented in this study evaluate the impact of the delivery pressure on the liquefaction cost, future work will also integrate these results with the shipping part of the chain (buffer

This is the accepted version of an article published in International Journal of Refrigeration
DOI: 10.1016/j.ijrefrig.2019.04.011

storage, ship transport and reconditioning), in order to identify the optimal transport conditions, as the transport pressure will also affect the shipping cost.

Acknowledgements
This publication has been produced with support from the NCCS Centre, performed under the Norwegian research program Centres for Environment-friendly Energy Research (FME). The authors acknowledge the following partners for their contributions: Aker Solutions, ANSALDO Energia, CoorsTek Membrane Sciences, Gassco, KROHNE, Larvik Shipping, Norcem, Norwegian Oil and Gas, Quad Geometrics, Shell, Statoil, TOTAL, and the Research Council of Norway (257579/E20).

References
Ahrends, J., Baehr, H.D., 1979. Die Thermodynamische Eigenschaften von Ammoniak. VDI-Verlag, Dusseldorf.
Anantharaman, R., Bolland, O., Booth, N., Dorst, E.V., Ekstrom, C., Franco, F., Macchi, E., Manzolini, G., Nikolic, D., Pfeffer, A., Prins, M., Rezvani, S., Robinson, L., 2011. D1.4.3 European best practice guidelines for assessment of CO_2 capture technologies (DECARBit Project). Available from: https://www.sintef.no/globalassets/project/decarbit/d-1-4-3_euro_bp_guid_for_ass_co2_cap_tech_280211.pdf.
Aspelund, A., Tveit, S.P., Gundersen, T., 2009. A liquefied energy chain for transport and utilization of natural gas for power production with CO2 capture and storage – Part 3: The combined carrier and onshore storage. Applied Energy 86, 805-814.
Berstad, D., Anantharaman, R., Nekså, P., 2013. Low-temperature CO_2 capture technologies – Applications and potential. International Journal of Refrigeration 36, 1403-1416.
Branan, C., 2005. Separators/Accumulators, Rules of thumb for chemical engineers: a manual of quick, accurate solutions to everyday process engineering problems, 4th ed. Elsevier.
Brunsvold, A., Jakobsen, J.P., Mazzetti, M.J., Skaugen, G., Hammer, M., Eickhoff, C., Neele, F., 2016. Key findings and recommendations from the IMPACTS project. International Journal of Greenhouse Gas Control 54, Part 2, 588-598.
Decarre, S., Berthiaud, J., Butin, N., Guillaume-Combecave, J.-L., 2010. CO2 maritime transportation. International Journal of Greenhouse Gas Control 4, 857-864.
Geske, J., Berghout, N., van den Broek, M., 2015. Cost-effective balance between CO_2 vessel and pipeline transport. Part I – Impact of optimally sized vessels and fleets. International Journal of Greenhouse Gas Control 36, 175-188.
Herzog, H., 2011. Scaling up carbon dioxide capture and storage: From megatons to gigatons. Energy Economics 33, 597-604.
Husebye, J., Brunsvold, A.L., Roussanaly, S., Zhang, X., 2012. Techno economic evaluation of amine based CO_2 capture: impact of CO_2 concentration and steam supply. Energy Procedia 23, 381-390.
IEAGHG, 2013. Deployment of CCS in the Cement industry.
IEAGHG, 2017. Feasibility Study for Ship Based Transport of Ethane to Europe and Back Hauling of CO_2 to the USA. Report 2017-TR1.
International Energy Agency, 2013. Technology Roadmap: Carbon capture and storage.
International Energy Agency, 2016. 20 years of Carbon Capture and Storage: Accelerating future deployment
Knoope, M.M.J., Ramírez, A., Faaij, A.P.C., 2015a. The influence of uncertainty in the development of a CO_2 infrastructure network. Applied Energy 158, 332-347.
Knoope, M.M.J., Ramírez, A., Faaij, A.P.C., 2015b. Investing in CO_2 transport infrastructure under uncertainty: A comparison between ships and pipelines. International Journal of Greenhouse Gas Control 41, 174-193.
Lindqvist, K., Roussanaly, S., Anantharaman, R., 2014. Multi-stage Membrane Processes for CO_2 Capture from Cement Industry. Energy Procedia 63, 6476-6483.
Ministry of Petroleum and Energy, 2016. Feasibility study for full-scale CCS in Norway. Available from https://www.gassnova.no/en/Documents/Feasibilitystudy_fullscale_CCS_Norway_2016.pdf.

This is the accepted version of an article published in International Journal of Refrigeration
DOI: 10.1016/j.ijrefrig.2019.04.011

Mota-Martinez, M.T., Hallett, J.P., Mac Dowell, N., 2017. Solvent selection and design for CO_2 capture - how we might have been missing the point. Sustainable Energy & Fuels 1, 2078-2090.
NETL, 2011. Quality guidelines for energy system studies: Cost estimation methodology for NETL assessments of power plant performance. DOE/NETL-2011/1455.
Peng, D.-Y., Robinson, D.B., 1976. New two-constant equation of state. Ind Eng Chem Fundam 15, 59-64.
Porter, R.T.J., Mahgerefteh, H., Brown, S., Martynov, S., Collard, A., Woolley, R.M., Fairweather, M., Falle, S.A.E.G., Wareing, C.J., Nikolaidis, I.K., Boulougouris, G.C., Peristeras, L.D., Tsangaris, D.M., Economou, I.G., Salvador, C., Zanganeh, K., Wigston, A., Najafali, J.N., Shafeen, A., Beigzadeh, A., Farret, R., Gombert, P., Hebrard, J., Proust, C., Ceroni, A., Flauw, Y., Zhang, Y., Chen, S., Yu, J., Talemi, R.H., Bensabat, J., Wolf, J.L., Rebscher, D., Niemi, A., Jung, B., Dowell, N.M., Shah, N., Kolster, C., Mechleri, E., Krevor, S., 2016. Techno-economic assessment of CO_2 quality effect on its storage and transport: CO_2QUEST: An overview of aims, objectives and main findings. International Journal of Greenhouse Gas Control 54, Part 2, 662-681.
Roussanaly, S., Anantharaman, R., 2017. Cost-optimal CO_2 capture ratio for membrane-based capture from different CO_2 sources. Chemical Engineering Journal 327, 618-628.
Roussanaly, S., Anantharaman, R., Lindqvist, K., Hagen, B., 2018. A new approach to the identification of high-potential materials for cost-efficient membrane-based post-combustion CO2 capture. Sustainable Energy & Fuels 2, 1225-1243.
Roussanaly, S., Brunsvold, A.L., Hognes, E.S., 2014. Benchmarking of CO_2 transport technologies: Part II – Offshore pipeline and shipping to an offshore site. International Journal of Greenhouse Gas Control 28, 283-299.
Roussanaly, S., Bureau-Cauchois, G., Husebye, J., 2013a. Costs benchmark of CO_2 transport technologies for a group of various size industries. International Journal of Greenhouse Gas control 12C, 341–350.
Roussanaly, S., Jakobsen, J.P., Hognes, E.H., Brunsvold, A.L., 2013b. Benchmarking of CO_2 transport technologies: Part I—Onshore pipeline and shipping between two onshore areas. International Journal of Greenhouse Gas Control 19, 584-594.
Roussanaly, S., Skaugen, G., Aasen, A., Jakobsen, J., Vesely, L., 2017. Techno-economic evaluation of CO2 transport from a lignite-fired IGCC plant in the Czech Republic. International Journal of Greenhouse Gas Control 65, 235-250.
Roussanaly, S., Vitvarova, M., Anantharaman, R., Berstad, D., Hagen, B., Jakobsen, J., Novotny, V., Skaugen, G., 2019. Cost comparison of technologies for pre-combustion CO_2 capture from a lignite-fired IGCC. Submitted to Frontiers of Chemical Science and Engineering.
Schittkowski, K., 1986. NLPQL: A fortran subroutine solving constrained nonlinear programming problems. Annals of Operations Research 5, 485-500.
Seo, Y., Huh, C., Lee, S., Chang, D., 2016. Comparison of CO_2 liquefaction pressures for ship-based carbon capture and storage (CCS) chain. International Journal of Greenhouse Gas Control 52, 1-12.
Skaugen, G., Roussanaly, S., Jakobsen, J., Brunsvold, A., 2016. Techno-economic evaluation of the effects of impurities on conditioning and transport of CO_2 by pipeline. International Journal of Greenhouse Gas Control 54, Part 2, 627-639.
Span, R., Wagner, W., 1996. A New Equation of State for Carbon Dioxide Covering the Fluid Region from the Triple-Point Temperature to 1100 K at Pressures up to 800 MPa. Journal of Physical and Chemical Reference Data 25, 1509-1596.
Størset, S.Ø., Tangen, G., Berstad, D., Eliasson, P., Hoff, K.A., Langørgen, Ø., Munkejord, S.T., Roussanaly, S., Torsæter, M., 2019. Profiting from CCS innovations: A study to measure potential value creation from CCS research and development. International Journal of Greenhouse Gas Control 83, 208-215.
Voldsund, M., Gardarsdottir, S.O., De Lena, E., Pérez-Calvo, J.-F., Jamali, A., Berstad, D., Fu, C., Romano, M., Roussanaly, S., Anantharaman, R., Hoppe, H., Sutter, D., Mazzotti, M., Gazzani, M., Cinti, G., Jordal, K., 2019. Comparison of Technologies for CO2 Capture from Cement Production—Part 1: Technical Evaluation. Energies 12, 559.

This is the accepted version of an article published in International Journal of Refrigeration
DOI: 10.1016/j.ijrefrig.2019.04.011

This is the accepted version of an article published in International Journal of Refrigeration
DOI: 10.1016/j.ijrefrig.2019.04.011

Appendix A : Cost model for the individual components of the CO_2 liquefaction process

In order to optimise process design to minimise the complete CO_2 liquefaction cost, direct cost models for each of the components of the liquefaction process were developed.
For each component, direct cost functions were regressed, using DataFit, based on several component cost evaluations performed with the Aspen Process Economic Analyzer. In order to ensure that the developed cost functions are valid for the conditions encountered in the optimisation model, a wide range of key component characteristics were carefully selected for each piece of equipment considered.

The following paragraphs document how these direct cost functions were developed including the adjusted coefficient of multiple determination (Ra^2), average absolute error (av. abs. error), and maximum absolute error (max. abs. error).

It is worth noting that even tough design margins, as recommended by Anantharaman et al. (Anantharaman et al., 2011), are included in evaluations of the direct costs of process component, the regressions are always related to the operating conditions (i.e. without design margin).

A.1 Compressors

In order to take the wide range of characteristics expected for the different compression stages into account, cost evaluation of 138 compressor stages was performed. Based on the outcome of different regressions, it found that developing a cost function specific to each compressor stage of the process would be significantly more accurate than developing a generic cost function applicable to all compressors.
For the compression stages of the CO_2 compression train and the refrigeration cycle, the regressions show that Eq. A.1 provides good fit for all the stages except for the fourth CO_2 compression stage, which is better modelled by Eq. A.2. The obtained regression parameters and characteristics for these six compression stages are summarised in Table A.1, while the regressions are plotted in Figure A.1.
Due to the specificity of the recirculation compressor and the wide range of possible characteristics, a more complex cost function, presented in Eq. A.3, is selected. The obtained regression parameters and characteristics of the recirculation compressor are summarised in Table A.2, while the regression is plotted in Figure A.1.

$$\text{Compressor direct cost [€]} = a + b \cdot (\text{Power [kW]})^{1.5} + c \cdot (\text{Power [kW]})^{2} \quad \text{(Eq. A.1)}$$

$$\text{Compressor direct cost [€]} = a + b \cdot (\text{Power [kW]}) + c \cdot (\text{Power [kW]})^{0.5} \quad \text{(Eq. A.2)}$$

$$\text{Compressor direct cost [€]} = a \cdot \text{Power [kW]} + b \cdot \text{Inlet Pressure [bar]} + c \cdot \text{Pressure ratio [-]} + d \quad \text{(Eq. A.3)}$$

Table A.1: Characteristics of the regression of the direct cost of the compressor stages of the CO_2 compression train and the refrigeration cycle

Parameter	CO_2 compression stages				Refrigeration cycle	
	Stage 1	Stage 2	Stage 3	Stage 4	Stage 1	Stage 2
Equation number	5	5	5	6	5	5
Coefficient a	831,732	1,040,305	1,316,807	1,168,183	736,639	889,060
Coefficient b	77.08	17.85	1.78	-51.28	79.91	28.24
Coefficient c	-0.676	-0.101	0.0223	16,476	-0.769	-0.255
Number of cases considered	10	9	9	12	11	11
Ra^2	0.988	0.987	0.981	0.996	0.990	0.994
Av. abs. error [%]	4.5	4.3	2.1	0.5	6.2	3.3
Max. abs. error [%]	10.4	8.9	4.0	1.6	12.6	7.8
Power range considered [kW]	350-5,000	400-5,000	400-5,000	200-5,000	250-5,000	300-5,000

This is the accepted version of an article published in International Journal of Refrigeration
DOI: 10.1016/j.ijrefrig.2019.04.011

Table A.2: Characteristics of the regression of the direct cost of the compressor stages of the recirculation compressor

Parameter	Value
Equation number	7
Coefficient a	287.2
Coefficient b	270
Coefficient c	29,439
Coefficient d	952,751
Number of cases considered	76
Ra^2	0.920
Av. abs. error [%]	3.7
Max. abs. error [%]	16.4
Power range considered [kW]	50-2,000
Inlet pressure range considered [bar]	6.5-45
Pressure ratio range considered [-]	1.3-9.2

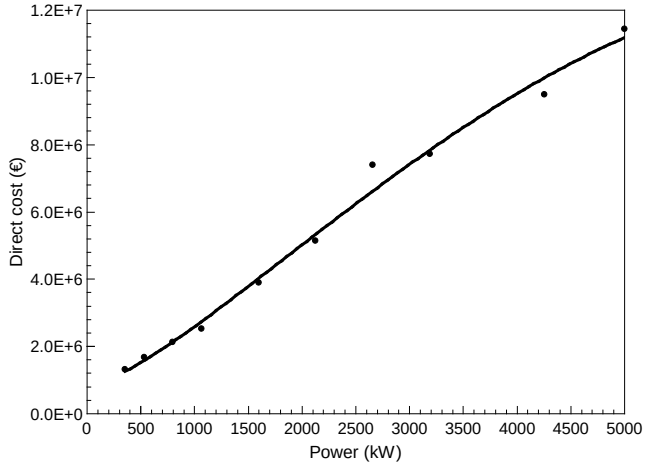

(a) CO_2 compressor stage 1

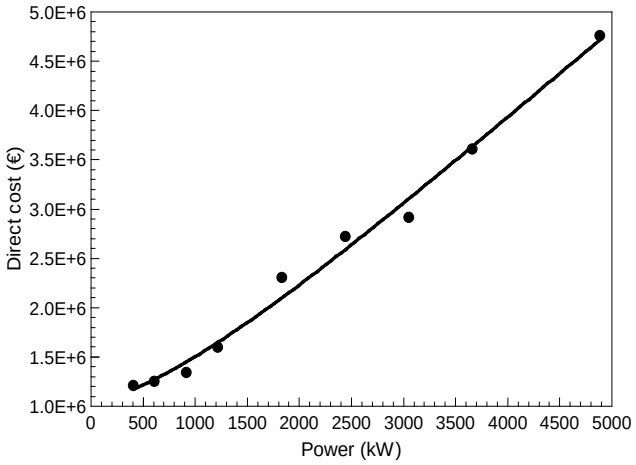

(b) CO_2 compressor stage 2

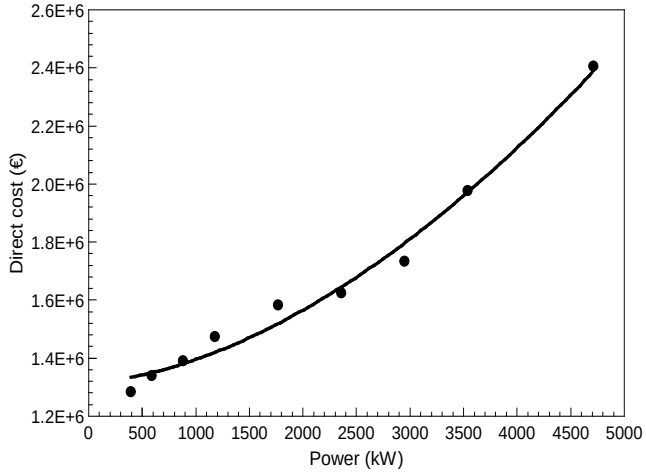

(c) CO_2 compressor stage 3

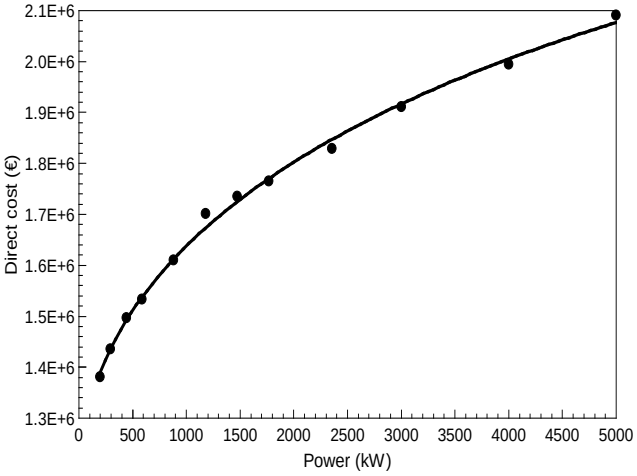

(d) CO_2 compressor stage 4

This is the accepted version of an article published in International Journal of Refrigeration
DOI: 10.1016/j.ijrefrig.2019.04.011

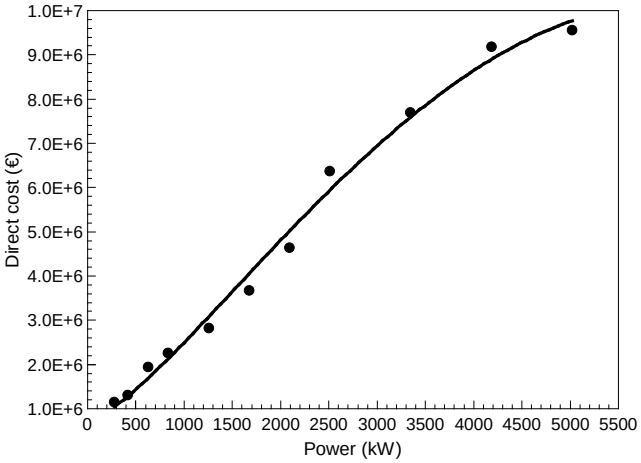

(e) Refrigeration cycle stage 1

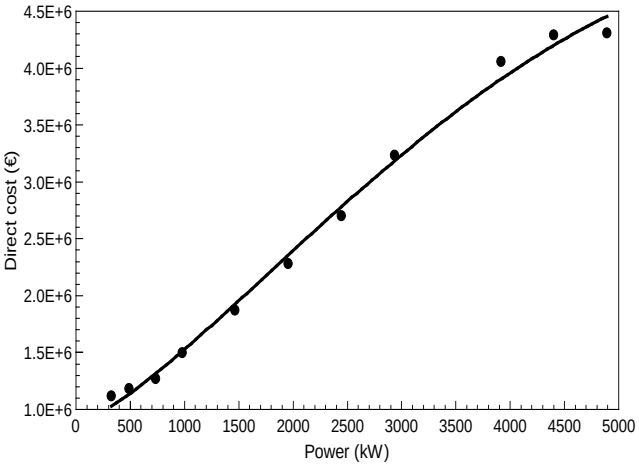

(f) Refrigeration cycle stage 2

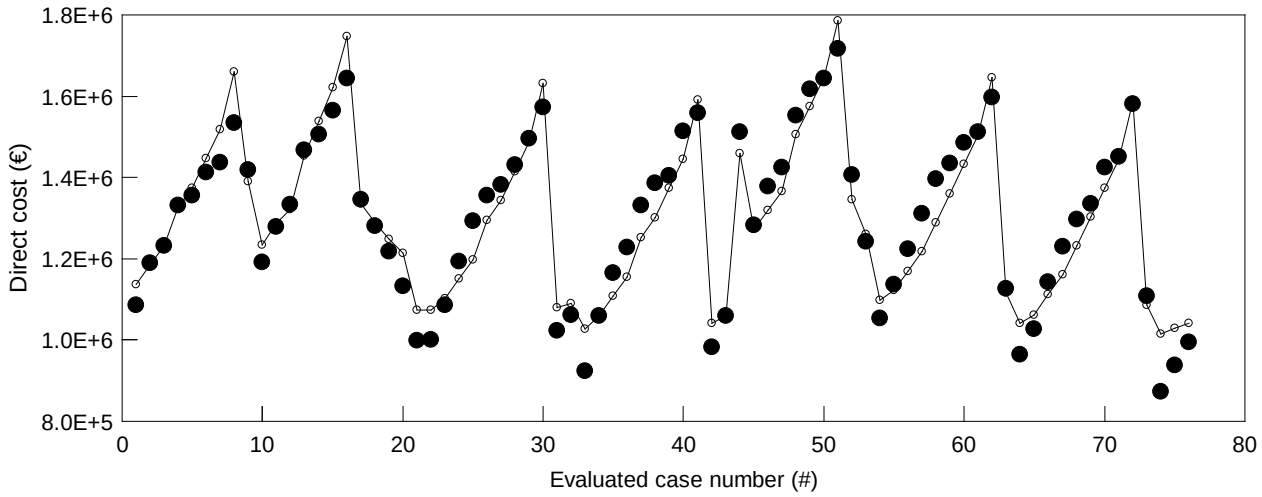

(g) Recirculation compressor

Legend: Evaluated direct cost — Regressed cost function

Figure A.1: Direct cost regressions for the different compressor stages of the CO_2 compression train, refrigeration cycle, and recirculation compressor

A.2 Heat exchanger

In order to establish a reliable cost function for the heat exchangers of the process, 53 heat exchangers with different heat exchange areas and pressures were evaluated as basis for the regression. A two-variables cost function, presented in Eq. A.4, was found to be suitable and representative of the different heat exchangers of the process. The obtained regression parameters and characteristics can be found in Table A.3, while the regression is plotted in Figure A.2.

$$\text{Heat exchanger direct cost [€]} = a \cdot (\text{Area [m}^2\text{]})^b \cdot c^{\text{Pressure [bar]}} \qquad \text{(Eq. A.4)}$$

Table A.3: Characteristics of the regression of direct cost of heat exchangers and flash tanks

Parameter	Heat exchanger	Flash tank
Equation number	4	5
Coefficient a	12,003	70,693
Coefficient b	0.603	0.562
Coefficient c	1.011187	1.015215
Number of cases considered	53	56
Ra^2	0.959	0.979
Av. abs. error [%]	14.2	6
Max. abs. error [%]	32.6	19.7
Area range considered [m^2]	30-4,000	2.5-60
Pressure range considered [bar]	2.7-81	5-70

This is the accepted version of an article published in International Journal of Refrigeration
DOI: 10.1016/j.ijrefrig.2019.04.011

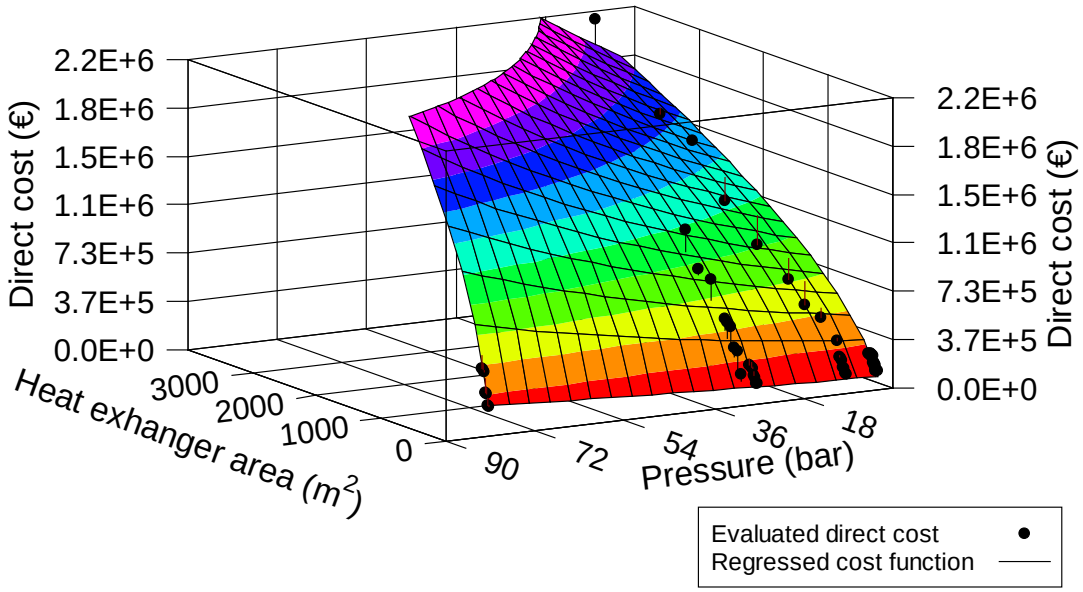

Figure A.2: Direct cost regression of heat exchangers

A.3 Flash separator

Based on an evaluation of 56 flash vessels, a two-variables equation, presented in Eq. A.5, was selected to be representative of the direct cost of a flash tank. The obtained regression parameters and characteristics can be found in Table A.3, while the regression is plotted in Figure A.3.

$$\text{Flash direct cost [€]} = a \cdot (\text{Volume [m}^3\text{]})^b \cdot c^{\text{Pressure [bar]}} \qquad \text{(Eq. A.5)}$$

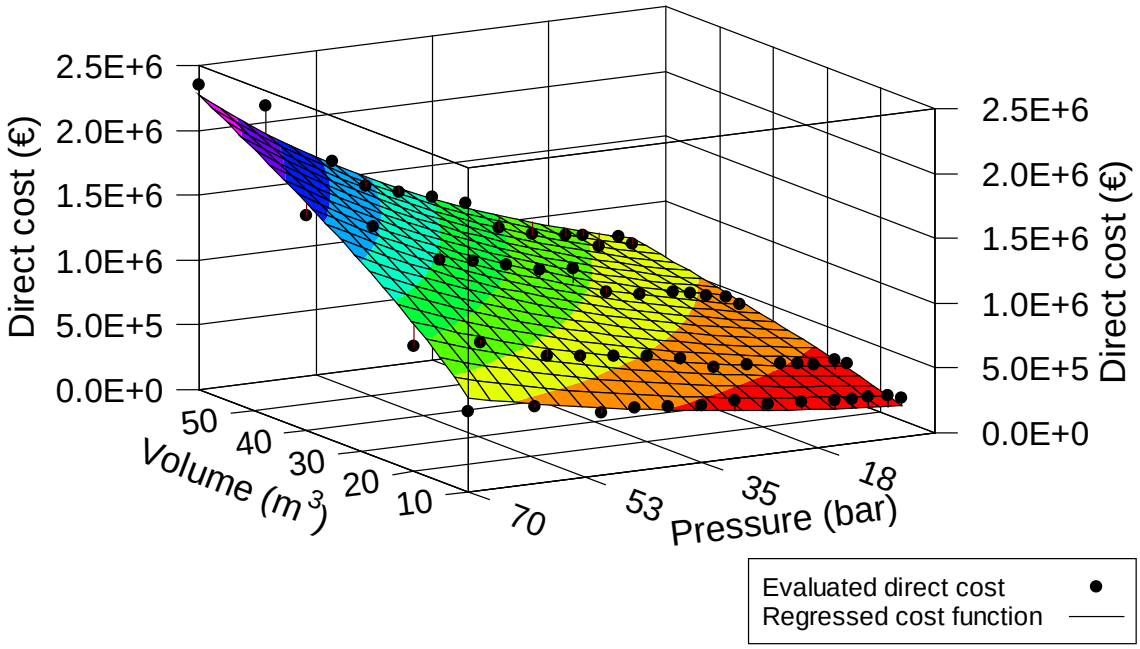

Figure A.3: Direct cost regression of flash separator

A.4 Dehydration

For cases in which the CO_2 stream after the CO_2 compression train must be further dehydrated to prevent ice formation during the liquefaction process, dehydration based on molecular sieves is considered. Following the design and evaluation recommendations of Anantharaman et al.

This is the accepted version of an article published in International Journal of Refrigeration
DOI: 10.1016/j.ijrefrig.2019.04.011

(Anantharaman et al., 2018) for molecular sieve dehydration, it was found that the direct cost of a molecular sieve could be scaled linearly to the amount of water to be removed, as shown in Eq. A.6.

$$\text{Molecular sieve direct cost [€]} = 90 \cdot \text{Removed water mass flow [kg.h}^{-1}\text{]} \qquad \text{Eq. A.6}$$

Appendix B : Key characteristics and cost breakdown of the CO_2 liquefaction for the different cases considered

B.1 Pure CO_2 case

Table B.1: Breakdown of the CO_2 liquefaction cost in function of the delivery CO_2 pressure post-liquefaction for the pure CO_2 case

Delivery CO_2 pressure post-liquefaction [bar]	7 bar	10 bar	15 bar	20 bar	25 bar	30 bar	40 bar	50 bar	60 bar	70 bar
Compression power [MW]	13.2	12.7	12.2	12.0	11.7	11.9	11.5	11.7	11.9	12.1
Cooling power [MW]	43.3	41.4	39.1	37.3	35.5	34.0	31.3	29.0	26.1	22.2
CO_2 recovery [%]	100	100	100	100	100	100	100	100	100	100
CO_2 purity [%]	100	100	100	100	100	100	100	100	100	100
CAPEX [€.tCO_2^{-1}]	4.8	4.7	4.3	4.1	4.1	4.0	3.9	3.9	3.9	3.9
Fixed OPEX [€.tCO_2^{-1}]	2.8	2.7	2.5	2.4	2.4	2.4	2.3	2.3	2.3	2.3
Electricity [€.tCO_2^{-1}]	9.5	9.2	8.6	8.4	8.3	8.2	8.1	8.2	8.4	8.6
Cooling water [€.tCO_2^{-1}]	0.5	0.5	0.6	0.5	0.5	0.5	0.4	0.4	0.3	0.3
Impurity removal [€.tCO_2^{-1}]	0	0	0	0	0	0	0	0	0	0
Purge cost [€.tCO_2^{-1}]	0	0	0	0	0	0	0	0	0	0
Total [€.tCO_2^{-1}]	17.7	17.1	16.0	15.3	15.2	15.0	14.7	14.7	14.8	15.1

B.2 Impurity cases

Table B.2: Breakdown of the CO_2 liquefaction cost in function of the delivery CO_2 pressure post-liquefaction in the case of amine-based post-combustion CO_2 capture from a cement plant

Delivery CO_2 pressure post-liquefaction [bar]	7 bar	10 bar	15 bar	20 bar	25 bar	30 bar	40 bar	50 bar	60 bar	70 bar
Compression power [MW]	13.5	13.0	12.4	12.0	11.8	11.6	11.5	11.5	11.7	12.0
Cooling power [MW]	44.2	42.5	40.2	38.2	36.6	35.0	32.2	29.6	27.4	22.2
CO_2 recovery [%]	97.8	98.0	98.4	98.4	98.3	98.3	98.3	98.3	98.3	98.3
CO_2 purity [%]	99.94	99.90	99.85	99.86	99.86	99.86	99.86	99.86	99.86	99.86
CAPEX [€.tCO_2^{-1}]	4.3	4.3	4.1	4.0	4.1	4.1	4.0	4.0	4.0	3.9
Fixed OPEX [€.tCO_2^{-1}]	2.6	2.6	2.4	2.4	2.4	2.5	2.4	2.4	2.4	2.3
Electricity [€.tCO_2^{-1}]	9.3	9.0	8.6	8.4	8.4	8.5	8.2	8.2	8.4	8.6
Cooling water [€.tCO_2^{-1}]	0.6	0.6	0.5	0.5	0.5	0.5	0.4	0.4	0.3	0.2
Impurity removal [€.tCO_2^{-1}]	0.1	0.1	0.1	0.1	0.0	0.0	0.0	0.0	0.0	0.0
Purge cost [€.tCO_2^{-1}]	1.1	0.9	0.8	0.6	0.5	0.3	0.3	0.3	0.3	0.3
Total [€.tCO_2^{-1}]	18.0	17.4	16.5	16.0	15.9	16.0	15.3	15.3	15.4	15.4

Table B.3: Breakdown of the CO_2 liquefaction cost in function of the delivery CO_2 pressure post-liquefaction in the case of membrane-based post-combustion CO_2 capture from a refinery

Delivery CO_2 pressure post-liquefaction [bar]	7 bar	10 bar	15 bar	20 bar	25 bar	30 bar	40 bar	50 bar	60 bar	70 bar
Compression power [MW]	15.1	15.1	14.3	14.0	13.7	13.1	12.3	12.1	12.4	12.2
Cooling power [MW]	45.0	44.2	42.3	41.1	40.1	38.3	34.4	31.2	24.8	21.2
CO_2 recovery [%]	95.9	96.6	96.9	97.9	98.8	99.5	99.5	99.5	99.5	99.5
CO_2 purity [%]	99.81	99.60	99.18	98.69	98.22	97.96	97.97	97.97	97.98	97.98
CAPEX [€.tCO_2^{-1}]	4.7	4.7	4.5	4.4	4.5	4.3	4.1	4.0	3.9	3.9
Fixed OPEX [€.tCO_2^{-1}]	2.8	2.8	2.7	2.6	2.6	2.6	2.4	2.4	2.3	2.3
Electricity [€.tCO_2^{-1}]	10.7	10.7	10.1	9.9	9.7	9.3	8.7	8.6	8.8	8.7
Cooling water [€.tCO_2^{-1}]	0.6	0.5	0.6	0.5	0.5	0.5	0.4	0.3	0.2	0.2

This is the accepted version of an article published in International Journal of Refrigeration
DOI: 10.1016/j.ijrefrig.2019.04.011

Impurity removal [€.tCO_2^{-1}]	0.1	0.1	0.1	0.1	0.0	0.0	0.0	0.0	0.0	0.0
Purge cost [€.tCO_2^{-1}]	1.2	1.0	0.9	0.7	0.5	0.3	0.3	0.3	0.3	0.3
Total [€.tCO_2^{-1}]	20.1	19.8	18.9	18.2	17.9	17.1	16.0	15.6	15.6	15.5

Table B.4: Breakdown of the CO_2 liquefaction cost in function of the delivery CO_2 pressure post-liquefaction in the case of rectisol-based pre-combustion CO_2 capture from a coal power plant

Delivery CO_2 pressure post-liquefaction [bar]	7 bar	10 bar	15 bar	20 bar	25 bar	30 bar	40 bar	50 bar	60 bar	70 bar
Compression power [MW]	14.8	14.1	13.7	13.4	13.2	12.8	12.2	12.3	12.3	12.2
Cooling power [MW]	45.1	43.2	41.4	40.7	39.2	37.9	34.3	27.5	22.6	21.5
CO_2 recovery [%]	97.4	97.4	97.7	98.4	98.9	99.6	100.0	100.0	100.0	100.0
CO_2 purity [%]	99.33	99.27	99.10	98.83	98.69	98.51	98.41	98.42	98.41	98.42
CAPEX [€.tCO_2^{-1}]	4.4	4.3	4.4	4.3	4.2	4.1	4.0	3.8	3.8	3.8
Fixed OPEX [€.tCO_2^{-1}]	2.6	2.5	2.6	2.5	2.5	2.4	2.3	2.2	2.2	2.2
Electricity [€.tCO_2^{-1}]	10.2	9.8	9.5	9.3	9.3	9.0	8.8	8.6	8.6	8.6
Cooling water [€.tCO_2^{-1}]	0.6	0.6	0.6	0.5	0.5	0.5	0.9	0.3	0.2	0.2
Impurity removal [€.tCO_2^{-1}]	0.0	0.0	0.0	0.0	0.0	0.0	0.0	0.0	0.0	0.0
Purge cost [€.tCO_2^{-1}]	1.1	0.9	0.9	0.7	0.5	0.3	0.3	0.3	0.3	0.3
Total [€.tCO_2^{-1}]	18.9	18.2	17.9	17.3	17.0	16.5	16.4	15.2	15.1	15.1

B.3 Impact of CO_2 purity constraint on the cost of CO_2 liquefaction in the case of membrane-based post-combustion CO_2 capture from a refinery

Table B.5: CO_2 liquefaction cost [€.tCO_2^{-1}] in function of the delivery CO_2 pressure post-liquefaction for different purity requirements in the case of membrane-based post-combustion CO_2 capture from a refinery

Delivery CO_2 pressure post-liquefaction [bar]	7 bar	10 bar	15 bar	20 bar	25 bar	30 bar	40 bar	50 bar	60 bar	70 bar
Pure CO_2 case	15.2	14.6	14.1	13.8	13.9	13.7	13.5	13.4	13.5	13.7
No purity constraint	20.1	19.5	18.5	17.4	16.7	15.6	14.6	14.2	14.2	14.1
>99% purity - solely with purge	20.0	19.4	18.4	17.8	17.9	-	-	-	-	-
>99% purity - impurity removal cost 300€/t	-	-	-	-	17.9	16.0	15.5	15.4	15.5	15.5
>99% purity - impurity removal cost 400€/t	-	-	-	-	17.9	16.7	16.2	16.1	16.2	16.1
>99% purity - impurity removal cost 500€/t	-	-	-	-	17.9	17.4	16.9	16.8	16.9	16.8
>99% purity - solely with purge	-	-	-	-	-	-	-	-	-	-
>99% purity - impurity removal cost 300€/t	20.9	19.7	19.3	18.4	18.2	18.0	17.8	17.7	17.8	17.7
>99% purity - impurity removal cost 400€/t	22.2	20.9	20.6	19.7	19.5	19.3	19.0	18.9	19.0	19.0
>99% purity - impurity removal cost 500€/t	23.5	22.2	21.8	20.9	20.7	20.5	20.3	20.2	20.3	20.2

This is the accepted version of an article published in International Journal of Refrigeration
DOI: 10.1016/j.ijrefrig.2019.04.011